Journal for ImmunoTherapy of Cancer

Pancreatic cancer cells escape T/NK cell immune surveillance through the expressional separation of CD58

Yalu Zhang,[1,2] Huaijin Zheng ,[2] Ronghua Zhang,[3,4] Jiayi Li,[2] Sen Yang,[2] Yuze Hua,[2] Jorg Kleeff,[5] Quan Liao,[2] Qiaofei Liu[2]

To cite: Zhang Y, Zheng H, Zhang R, *et al*. Pancreatic cancer cells escape T/NK cell immune surveillance through the expressional separation of CD58. *Journal for ImmunoTherapy of Cancer* 2025;**13**:e012163. doi:10.1136/jitc-2025-012163

► Additional supplemental material is published online only. To view, please visit the journal online (https://doi.org/10.1136/jitc-2025-012163).

YZ, HZ and RZ are joint first authors.

Accepted 29 August 2025

For numbered affiliations see end of article.

Correspondence to
Prof Qiaofei Liu;
qfliu@aliyun.com

Prof. Quan Liao;
lqpumc@126.com

ABSTRACT

Background Membrane (m) CD58 is a co-stimulatory ligand that binds to CD2, and the CD2-(m) CD58 axis participates in lymphocyte activation. In addition to mCD58, a soluble form of CD58 (sCD58) has been reported in human serum, urine, and in vitro cell culture supernatants. The role of sCD58 in the tumor immune microenvironment of pancreatic ductal adenocarcinoma (PDAC) is currently unknown.

Methods The expression and prognostic role of CD58 in PDAC tissues were analyzed using various public databases. Then, the phenomenon of expressional separation of CD58 in PDAC cells induced by macrophages was observed by flow cytometry and ELISA, where the decrease of mCD58 on the membrane surface is accompanied by the increase of sCD58 in the supernatant. The molecular mechanisms of the expressional separation of CD58 were further explored by focusing on the TGF-β signaling pathway. The effects of expressional separation of CD58 on the immune activity and killing ability of T/NK cells for PDAC were determined in co-culture models. Furthermore, subcutaneous tumor-bearing models, lung metastasis models, and intraperitoneal dissemination models were used to confirm the in vitro data. Finally, the diagnostic and prognostic roles of serum sCD58 were determined by using 561 samples from PDAC patients, benign pancreatic disease patients, and healthy controls.

Results Elevated CD58 expression in PDAC tissues was associated with worse clinical outcomes. After co-culture with PDAC cells, macrophages adopted an M2 phenotype, characterized by a high expression level of TGF-β. Co-cultured macrophages could induce the expressional separation of CD58 in PDAC cells. Activation of the TGF-β/Smad2/3 pathway markedly promoted this separation, and pathway inhibition largely blocked it. In vitro and in vivo assays revealed that mCD58 engaged CD2 on T/NK cells, facilitated their activation, enhanced their cytotoxicity, and stimulated the release of the anti-tumoral cytokines IFN-γ and TNF-α. Conversely, local high concentrations of sCD58 accumulation in PDAC tissues interfered with the CD2-CD58 axis by competitively binding CD2, inhibited the activation of T/NK cells, reduced T/NK cytotoxicity, and the secretion of IFN-γ and TNF-α. Furthermore, serum sCD58 levels were higher in the PDAC patients than in the healthy controls or patients with benign pancreatic diseases. sCD58 improved the diagnostic and prognostic power of CA199 in PDAC patients. A combined model incorporating CA199, TGF-β1, and sCD58 yielded an AUC (area under the curve) value of 0.946 for overall diagnosis. In the CA199 negative cohort, the combined model of TGF-β and sCD58 achieved an AUC of 0.955.

Conclusions This study uncovers a novel vicious crosstalk among macrophages, T/NK cells, and PDAC cells within the tumor microenvironment. Macrophages drive the expressional separation of CD58 via the TGF-β/Smad2/3 signaling pathway. This shift suppresses T/NK-cell activity, allows tumor cells to evade immune killing, and accelerates PDAC progression. In addition, serum sCD58 emerges as a promising diagnostic and prognostic biomarker for PDAC.

WHAT IS ALREADY KNOWN ON THIS TOPIC

⇒ Pancreatic ductal adenocarcinoma (PDAC) exhibits profound immunosuppression driven by tumor-associated macrophages (TAMs), yet the specific mechanisms by which TAMs disable T/NK-cell surveillance remain incompletely defined. Soluble CD58 (sCD58) exists in bodily fluids, but its role in PDAC immune evasion was previously unknown.

WHAT THIS STUDY ADDS

⇒ We identify a novel "expressional separation" of CD58 in tumor microenvironment of PDAC: TAM-derived TGF-β/Smad2/3 signaling induces reducing membrane CD58 (mCD58) while elevating sCD58, which competitively blocks CD2 on T/NK cells to suppress cytotoxicity and cytokine release, ultimately promoting the immune escape of PDAC cells. Besides, serum sCD58 levels correlate with tumor progression and synergize with CA19-9/TGF-β1 to diagnose PDAC.

HOW THIS STUDY MIGHT AFFECT RESEARCH, PRACTICE OR POLICY

⇒ Targeting the TGF-β/CD58 axis (eg, via sCD58 blockade or Smad inhibition) represents a new immunotherapeutic strategy to restore T/NK-cell function. The sCD58-based diagnostic model may significantly improve PDAC detection, particularly in CA19-9-negative patients.

INTRODUCTION

Pancreatic ductal adenocarcinoma (PDAC) is one of the most invasive and challenging malignancies, accounting for approximately 90% of all pancreatic cancers.[1] Due to the majority of patients being already in advanced stage when they are first diagnosed,

the mortality rate of PDAC patients is nearly equal to its incidence, with a postoperative 5-year survival rate of only 10%.[2 3] Therefore, it is urgent to find effective biomarker and therapeutic target for PDAC.

PDAC is characterized by a highly fibrotic and immunosuppressive tumor microenvironment (TME), where tumor cells constitute only ~30% of the lesion, while immune-inflammatory cells, particularly tumor-associated macrophages (TAMs), dominate the tumor immune microenvironment (TIME).[4–7] TAMs drive PDAC progression by suppressing antitumor immunity,[8 9] accelerating tumor angiogenesis,[10] disrupting the extracellular matrix to facilitate PDAC metastasis,[11] and promoting epithelial-mesenchymal transition.[12] CD40 agonists,[13] CCR2 inhibitors,[14] CD47 monoclonal antibodies (mAbs),[15] and CSF-1/CSF-2 mAbs[16] targeting TAMs have demonstrated therapeutic effects in PDAC animal models. Although high $CD8^+$ T cell infiltration is linked to better prognosis,[17] immune checkpoint blockade (ICB) remains ineffective as a monotherapy in PDAC.[18–21] Natural killer (NK) cells can rapidly recognize transformed cells and eliminate them directly or indirectly via cytokine secretion (eg, IL-6, IFN-γ, TNF, G-CSF), but they are frequently reprogrammed by the TME toward a pro-tumoral phenotype.[22 23] The impaired function of T/NK cells compromises antitumor immunity, and their crosstalk with TAMs further promotes immunosuppression by inducing regulatory T cells, disrupting T cell metabolism, impairing antigen presentation, and suppressing NK cell activity.[6 24 25] However, the detailed interplay between TAMs and T/NK cells within the TIME of PDAC remains largely unknown.

CD58, also known as lymphocyte function-associated antigen-3 (LFA-3), belongs to the immunoglobulin superfamily.[26] CD58 is a highly glycosylated cell adhesion molecule, widely distributed as a type I transmembrane or phosphatidylinositol-anchored form in hematopoietic and non-hematopoietic tissues.[27] CD2 is a surface glycoprotein limited to T cells, NK cells, thymocytes, and subsets of bone marrow cells.[28] CD2 is one of the most crucial adhesion receptors on almost all T lymphocytes and provides co-stimulatory signals after interacting with CD58 on target cells.[29 30] In addition to membrane-anchored CD58 (mCD58) expressed on cell membranes, a soluble form of CD58 (sCD58) has been reported to be present in human serum, urine, and in vitro cell culture supernatants.[31] However, the role of sCD58 in PDAC remains unclear.

This study delineated the roles, molecular mechanisms, and clinical significance of sCD58 in PDAC patients. We uncovered a novel interplay between TAMs and T/NK cells within the TIME of PDAC. TAMs could induce the expressional separation of CD58, resulting in elevated sCD58 and reduced mCD58 via TGF-β/Smad2/3 signaling. This process inhibited T/NK cell activity, weakened T/NK cell-mediated cytotoxicity, and accelerated PDAC progression. Clinically, serum circulating sCD58 improved the diagnostic and prognostic power of CA19-9.

MATERIALS AND METHODS

Data availability

The GEO database is a public gene-expression repository hosted by the National Center for Biotechnology Information. The datasets used during the current study are available from the following public databases: six GEO datasets were used to compare CD58 expression in PDAC tissues with either adjacent non-cancerous tissues (ANCTs) (GSE28735 and GSE15471) or normal pancreatic tissues (GSE62452, GSE16515, GSE62165, GSE71729). Besides, the GSE19650 dataset was used to investigate the expression of CD58 across different pancreatic low-grade malignant tumors. In the GSE51971 dataset, PDAC cells were stratified into triple-negative and triple-positive groups based on CD44, CD133, and EpCAM expression levels. All GEO datasets were analyzed using quantile normalization methods to ensure identical value distributions across all selected samples. UALCAN is a comprehensive and interactive web resource for cancer-omics analysis.[32] Here, the UALCAN database was used to compare CD58 transcript levels across different degrees of differentiation and tumor tissue with or without TP53 mutations. LinkedOmics is an integrated multiomics portal based on the mass-spectrometry data of the Clinical Proteomic Tumor Analysis Consortium.[33] In this study, LinkedOmics database was used to evaluate the overall survival in 172 PDAC patients stratified by high versus low CD58 expression.

Patients and samples

PDAC tissues and ANCTs were collected as previously described.[34] From September 2013 to January 2024, peripheral blood samples from routine clinical laboratory tests were collected from patients undergoing preoperative evaluation for pancreatic diseases at Peking Union Medical College Hospital and from individuals undergoing routine health examinations at the medical center in January 2022. Inclusion criteria: (1) older than 18 years old; (2) pathological diagnosis of pancreatic diseases. Exclusion criteria: (1) preoperative radiotherapy or chemotherapy; (2) autoimmune diseases, such as systemic lupus erythematosus, autoimmune thyroiditis; (3) inflammatory diseases, such as hepatitis, inflammatory bowel disease, rheumatoid arthritis; (4) hematological malignancies, such as acute/chronic leukemia, diffuse large B-cell lymphoma; and (5) refused to sign informed consent. A total of 516 peripheral blood serum samples were included, comprising 171 cases of PDAC, 132 cases of healthy controls, and 213 cases of benign pancreatic disease (chronic pancreatitis, pancreatic pseudocyst, solid pseudopapillary tumor of the pancreas, pancreatic serous cystadenoma, and pancreatic mucinous cystadenoma). All cases except healthy controls were pathologically diagnosed, and clinicopathological characteristics of the patients were collected. Furthermore, the age distribution and gender ratio of the healthy control group were ensured to be similar to or the same as those of the PDAC patients to eliminate differences caused by age and gender.

Cell culture and treatment

The human normal pancreatic ductal epithelial cell line (HPNE) and PDAC cell lines (Panc-1, AsPC-1, BxPC-3, Mia Paca-2, SW1990, CFPAC-1, KPC, Panc02), as well as the monocyte cell line THP-1, were all obtained from the National Infrastructure of Cell Line Resource of China Medical Science Academy and preserved in the Laboratory of General Surgery at Peking Union Medical College Hospital. Specifically, HPNE, Panc-1, and Mia Paca-2 cell lines were cultured in DMEM medium (Gibco, MA, USA), while THP-1, AsPC-1, and BxPC-3 cell lines were cultured in RPMI-1640 medium (Gibco, Massachusetts, USA). CFPAC-1 was cultured in IMDM medium (Hyclone, Utah, USA), and SW1990 was cultured in L-15 medium (Gibco). These culture media were supplemented with 10% fetal bovine serum (FBS) (Gibco) and 1% penicillin-streptomycin (PS) (Gibco). The murine PDAC cells Panc02 and KPC were cultured in DMEM medium (Gibco) containing 5% FBS and 1% PS. T/NK cells isolated from mouse splenocytes were cultured in RPMI-1640 medium (Gibco) containing 10% FBS and 1% PS. Normal pancreatic and PDAC cell lines were maintained in a humidified incubator at 37°C with 5% CO_2. The HPNE cell culture medium was also supplemented with an additional 10 ng/mL of recombinant human epidermal growth factor (P00033, Solarbio, China). Recombinant human TGF-β1 (5 ng/mL; ab50336, Abcam, UK) was used to activate the TGF-β/Smad2/3 pathway, while SB431542 (20 µM; ab120163, Abcam, UK) was applied to inhibit TGF-β receptor signaling. Recombinant human CD58 (ab179975, Abcam, UK) was used to mimic the effect of sCD58 on macrophages. Recombinant murine CD48 (3327-CD, R&D Systems, USA) was used to simulate the effect of sCD58 on murine T cell cytotoxicity. Recombinant anti-CD2 mAbs (ab219411, Abcam, UK) were used in blocking experiments within the co-culture system of T cells and tumor cells. Recombinant mouse TGF-β1 (15805, Cell Signaling Technology, USA) was administered to investigate the effects of TGF-β1 on PDAC tumor growth in vivo.

Indirect co-culture

The monocytic cell line THP-1 was induced to adhere by employing a final concentration of 100 ng/mL phorbol 12-myristate 13-acetate (PMA) (P8139, Sigma-Aldrich, USA). After 24 hours of induction, the cells adhered to become primary macrophages (M0). To analyze the influence of PDAC cells on macrophages, macrophages were seeded in the lower chamber of a Transwell plate (0.4 µm pore size; 3460, Corning, USA), while PDAC cells were seeded in the upper chamber. Conversely, to assess macrophage effects on PDAC cells, macrophages in the upper chamber, while PDAC cells in the lower chamber. Following a 72-hour co-culture period, PDAC cells and macrophages were separately collected for further analysis.

Plasmids, transfection, and lentivirus production

The lentiviral silencing vector targeting the human CD58 gene (NM_001779) and the lentiviral overexpression vector targeting the mouse CD48 gene (NM_007649) were synthesized by commissioning to Shanghai Genechem. The designed RNAi target sequence for gene silencing is as follows: 3'-TGGGATTGTCCTATGGAGCAA-5'. A cell suspension with a density of 4×10^4 cells/ml was prepared and seeded into culture dishes. The cells were incubated at 37°C for 16–24 hours until reaching a confluency of approximately 30%. Following this, the viral inoculum was infected with an appropriate volume, considering a Multiplicity of Infection of 10. The cells were further cultured for 16 hours, followed by a medium replacement. After 72 hours postinfection, stable cell lines were selected using 2 µg/mL puromycin. A dual-targeting siRNA (si-smad2/3) was designed against conserved sequences of human Smad2 and Smad3 by Guangzhou Ribobio Biotechnology. The sequence is as follows: 5'-TGAAGATCTTCAACAACCA-3'. A control group with a sequence provided and stored by the same company was used for comparison. The siRNA and its scrambled control were transfected using Lipofectamine 2000 transfection reagent (11668019, Invitrogen, California, USA) according to manufacturer's protocol.

HE, immunofluorescence staining, and immunohistochemical staining

The HE, immunofluorescence (IF), and immunohistochemical (IHC) staining were performed as described previously.[35] For IF, the tissue sections were fixed and stained with corresponding primary antibody and incubated with Alexa Fluor 488/546-labeled secondary antibody (Solarbio, China). Nuclei were treated with 4',6-diamidino-2-phenylindole (DAPI). The sections were photographed with an inverted fluorescence microscope (Olympus, Japan). The primary antibodies used were listed as follows: Human CD58 antibody (AF-1689, R&D Systems, USA); Mouse CD48 antibody (AF-3327, R&D systems, USA); Anti-CD206 antibody (24595, Cell Signaling Technology, USA); Anti-NKp46 antibody (ab208943, Abcam, UK); Anti-CD8 antibody (ab217344, Abcam, UK).

Western blotting

Total cell lysates were extracted in a 2% SDS lysis buffer containing a protein phosphatase inhibitor mixture (P1265, Applygen, China). About 30 µg of total protein was separated on 8% or 12% SDS-PAGE gels. After electrophoresis, proteins were transferred to nitrocellulose membranes (HATF00010, Millipore, Ireland) and blocked with 5% BSA-V (Solarbio, Beijing, China) for 1 hour at room temperature. Quality assessment was conducted with anti-GAPDH antibodies. The membrane was incubated overnight at 4°C with a primary antibody. Following three TBST washes, the membrane was incubated with an HRP-conjugated secondary antibody (Zsbio, Beijing, China) for 1 hour at room temperature (1:500 dilution). Visualization was achieved using an ECL reagent kit (P1050, Applygen, China) after three

additional TBST washes. The primary antibodies used are listed in online supplemental Table S1.

Quantitative real-time PCR

Total RNA was extracted from cells using TRIzol reagent (9108, Takara, Japan) as the manufacturer's instructions. Reverse transcription used the kit (RR037A, Takara, Japan), followed by quantitative real-time PCR with TB Green Premix Ex Taq (Tli RNaseH Plus) (RR420A, Takara, Japan). GAPDH served as the internal control, and data analysis employed the $2^{-\Delta\Delta CT}$ method. The primers and their sequences used in this study are shown in online supplemental Table S2.

Colony-formation and cell-proliferation assays

PDAC cells underwent digestion, centrifugation, resuspension, and counting. Equal cell numbers were seeded in 6-well plates, labeled by group, and cultured for 14 days. Visible colonies were fixed with 4% paraformaldehyde for 15 min and stained with 0.1% crystal violet for 15 min. Colony numbers were recorded after imaging. In terms of cell proliferation assays, cell suspensions were adjusted to 3×10^4 cells/mL, and 100 µl were seeded in each well of a 96-well plate (3000 cells/well). Triplicate biological replicates were performed for each group. After 4–6 hours of incubation at 37°C, allowing cell adhesion, 100 µL of 10% CCK-8 solution (CK04, DOJINDO, Japan) was added per well and incubated for 2 hours. Absorbance at 450 nm was measured using a microplate reader at 0 hours, 24 hours, 48 hours, and 72 hours, plotting results on a line graph.

Wound-healing assays

PDAC cells from experimental and control groups were harvested, digested, and centrifuged. The resulting cell pellets were resuspended in a complete medium, and cell counts were performed. Subsequently, 5×10^5 cells were seeded into each well of a six-well plate. The following day, a 200 µL pipette tip was used to create a straight scratch along a ruler on the cell monolayer. After gently washing with PBS, a serum-free medium was added to limit cell proliferation. The plate was then placed in the incubator, and microscopic observations were recorded at 24 hours intervals until complete closure of the scratch was achieved.

Transwell invasion assays

Matrigel, prechilled at 4°C, was diluted in a serum-free medium at a 9:1 ratio. A 100 µL of Matrigel dilution (356234, Corning, USA) (50 µl/cm²) was added to the upper chamber, allowing Matrigel to gel at 37°C. PDAC cells were digested, centrifuged, resuspended in serum-free medium, and counted. Before seeding, a 100 µl of the cell suspension was mixed with Matrigel in a serum-free medium. A 100 µL of the cell-Matrigel mixture was added to the upper chamber, while the lower chamber received 500 µL of medium containing 10% FBS. After 24 hours of incubation, the upper and lower chamber media were discarded, and PBS was used for washing. The lower chamber was fixed with 4% paraformaldehyde for 20 min and stained with 0.1% crystal violet for another 20 min. After discarding the staining solution and careful removal of excess Matrigel and non-invading cells on the upper surface using a moist cotton swab, microscopic observations were made. Five random fields were selected for cell counting, and images were captured.

Flow cytometry analysis

Cells were harvested by standard digestion, centrifugation, and resuspension in Cell Staining Buffer (420201, BioLegend, USA). The cell density was adjusted to $(3–8)\times10^5$ cells/mL, and each group received 1 mL of the cell suspension. For human cells, Fc receptors were blocked using 5 µL TruStain FcXTM (156603, BioLegend, USA) per 100 µL of cell suspension, followed by 10 min incubation at room temperature. After centrifugation, cells were incubated with an appropriate primary antibody on ice for 30 min. Following centrifugation and washing, cells were resuspended. After a 5 min incubation on ice, the samples were ready for flow cytometry analysis (FCM). The antibodies used are listed in online supplemental Table S3.

ELISA

The standard curve was prepared as per the kit instructions by diluting standards in EP tubes. Each assay included wells for test samples, standards, and blanks. Standard wells received 50 µL of accurate standard solutions, while test sample wells received 40 µL sample diluent and 10 µL diluted test sample. After incubation and washing steps, enzyme conjugate was added, followed by color developer A and B. The reaction was stopped with stop solution after a final incubation period. Absorbance was measured by an ELISA reader within 15 min of stopping the reaction. Standard equations derived from OD values and standard concentrations were used to determine sample concentrations, considering dilution factors, providing accurate final concentrations for the samples. The commercial kits used in this study were as follows: Human CD58 ELISA kit (MM-1518H1, Meimian, China); Human TGF-β1 ELISA kit (MM-0090H1, Meimian, China); Mouse IFN-γ ELISA Kit (MM-0182M1, Meimian, China); Mouse TNF-α ELISA Kit (MM-0132M1, Meimian, China); Mouse TGF-β1 ELISA Kit (MM-0135M1, Meimian, China).

T cell cytotoxicity assay

We activated murine T cells in vivo by heat-inactivating Panc02/KPC cells and co-administering them with Freund's adjuvant to C57BL/6 mice for 3 weeks. Spleen cells were harvested, processed into a single-cell suspension, and debris was removed. The effect of spleen cell debris removal is shown in online supplemental Figure 1A. T/NK cells were isolated using magnetic-activated cell sorting with anti-CD8a or anti-NK cell biotin-antibody cocktails. The final purity of the obtained T/NK cells consistently reached over 90% (online supplemental Figure 1B). T cells were then activated, expanded, and restimulated in vitro using Dynabeads Mouse T-Activator

CD3/CD28 kit (11 452D, Gibco, USA). Detailed procedures can be found in online supplemental Methods.

Lactate dehydrogenase release assay

The extracellular cytotoxicity of T cells was assessed using a commercial lactate dehydrogenase (LDH) Cytotoxicity Detection Kit (C0016, Beyotime, China). Briefly, cells were seeded in a 96-well cell culture plate to achieve approximately 80% confluence during the assay. The culture wells were divided into four groups: blank control wells, sample control wells, test sample wells, and wells for maximum enzyme activity control. 1 hour prior to the assay, the 96-well plate was carefully removed, and LDH release reagent was added to the wells designated for maximum enzyme activity control, constituting 10% of the original volume. The mixture was incubated for 1 hour, and 120 µL of the supernatant from each well was transferred to a new 96-well plate. Subsequently, 60 µL of the working solution was added according to the kit instructions. After thorough mixing, the plate was incubated in the dark for 30 min, and the absorbance was measured at 490 nm using a microplate reader. The cytotoxicity percentage was calculated as follows: Cytotoxicity (%)=(Absorbance of treated sample–Absorbance of sample control)/(Absorbance of maximum enzyme activity–Absorbance of sample control)×100.

DMBA-induced spontaneous PDAC murine models

The spontaneous PDAC model was established as described previously.[35] Mice were fasted for 6 hours before surgery. Anesthesia was induced by intraperitoneal injection of 1% sodium pentobarbital (50 mg/kg), followed by depilation of the left lateral rib area with 10% sulfur sodium and disinfection with 75% alcohol. A 1.5 cm incision was then made to expose the spleen and distal pancreas. A pocket with a 1 cm diameter was presewn at the distal of the pancreas end using CV-7 sutures. DMBA (Sigma-Aldrich D3254), a strong carcinogen, was carefully placed in the pocket at a dose of 1 mg per mouse, followed by suturing. The abdominal cavity was inspected for agent leakage before closure. After 2 months of postoperation, the mice were euthanized under anesthesia and pancreatic lesions were analyzed.

Subcutaneous tumor-bearing models

Murine PDAC cells were expanded at a quantity of 1×10^7 cells, maintaining a density of 80%. After standard cell digestion, centrifugation, and PBS resuspension, the cell concentration was adjusted to 1×10^8 cells/mL and stored at 4°C. C57BL/6 or NSG mice underwent subcutaneous inoculation in the right inguinal region with 100 µL of the cell suspension. The whole process is generally completed within 1 hour as far as possible to avoid affecting the cell viability. Mice in the rm-CD58 group received peritumoral injections of recombinant mouse CD48 (5 µg/mL) at a dose of 100 µL per mouse every 3–4 days. The TGF-β1-treated group was administered recombinant mouse TGF-β1 (100 ng/mL) on the same schedule. Body weight (g) and tumor volume (mm^3) were measured weekly. Tumor volume (V) was calculated ($V=length\times width^2\times0.5$), and growth curves were plotted. Mice were euthanized under anesthesia, and tumors were harvested, weighed, and photographed.

Single-cell digestion of tumor tissues

After weighing the tumor tissue (g), it was finely minced with surgical scissors and subjected to enzymatic digestion in a tissue digestion solution 10% FBS, 0.5 mg/mL collagenase IV (C5138, Sigma-Aldrich, USA), 0.15 mg/mL DNase I (DN25, Sigma-Aldrich, USA), RPMI-1640 at a volume five times that of the tissue. The digestion was carried out at 37°C in a water bath for 1 hour with gentle agitation every 10 min. Subsequently, the digested mixture was supplemented with an ample amount of complete culture medium, centrifuged to remove the supernatant, resuspended, and filtered through a 40 µm cell strainer to eliminate large tissue fragments. After adjusting the cell density to 1×10^7 cells/mL, the suspension was prepared for FCM.

Lung metastasis model in NSG mice

NSG immunodeficient mice were randomly divided into two groups (5 mice per group) and received Panc-1 cells transfected with sh-CD58 or sh-NC. The cells were resuspended in PBS at a density of 1×10^7 cells/mL. To minimize cell aggregation, the cell suspension was repeatedly pipetted before injection. The mice were restrained to expose the tail vein, wiped with 75% ethanol, and slowly injected with 100 µL of cell suspension into the tail vein per mouse. At 1 month after the injection, NSG mice were euthanized to harvest lung tissues for further analysis.

Intraperitoneal dissemination models

The right inguinal area of C57BL/6 mice was depilated with 10% sodium sulfide, followed by disinfection of the local skin with 75% alcohol. A well-mixed suspension of PDAC cells at a concentration of 2×10^7 cells/mL was promptly injected into the mouse peritoneal cavity using a disposable sterile syringe, delivering 500 µL per mouse.

Mice in the rmCD58-treated group received intraperitoneal injections of rmCD58 (5 µg/mouse) twice weekly. Following each injection, mice were appropriately shaken to fully diffuse the solution in the peritoneal cavity. After 2 weeks, mice were euthanized under anesthesia. A 2 mL PBS solution was injected into the peritoneal cavity, and the abdomen was massaged and shaken. Peritoneal lavage fluid was collected and stored in the prechilled tubes. After centrifugation, the supernatant was used for cytokine detection, while the precipitated cells were employed for flow cytometry staining.

Statistical analysis

Statistical analyses and graphical representations were performed using IBM SPSS Statistics V.21.0 (SPSS) or GraphPad Prism V.8.0 (La Jolla, California, USA). Statistical analyses were performed to compare groups based on the distribution of data. Parametric Student's *t* test

or non-parametric Mann-Whitney *U* test was chosen for two-group comparisons. For comparisons involving three or more groups, one-way analysis of variance or Kruskal-Wallis *H* test was used, followed by Dunnett-*t* or Tukey post hoc tests. Spearman or Pearson correlation analysis was used to assess linear correlations between variables according to different situations. Pearson's χ^2 test evaluated correlations between categorical variables. Diagnostic accuracy was evaluated using receiver operator characteristic curves (ROC) and the area under curve (AUC) values, with the optimal cut-off value determined by the maximum Youden index. Binary logistic regression (input) was used to develop dual-marker (sCD58+TGF-β1) and triple-marker (sCD58+TGF-β1+CA199) models. For dual-marker model: Y = 0.021326 × sCD58 (ng/mL) + 0.009186 × TGF-β1 (pg/mL) − 16.34. For triple-marker model: Y = 0.019531 × sCD58 (ng/mL) + 0.009493 × TGF-β1 (pg/mL) + 0.000953 × CA199 – 16.32. Survival analysis was conducted using the Kaplan-Meier method and log-rank test, with optimal survival cut-off values determined by X-tile software. Statistical significance was set at $p < 0.05$ (two-tailed).

RESULTS

CD58 is elevated in PDAC tissues and acts as an adverse prognostic factor

Transcriptomic analyses of GSE28735 and GSE15471 showed that CD58 mRNA levels were upregulated in PDAC tissues compared with paired ANCTs (figure 1A,B). Additional GEO datasets (GSE62452, GSE16515, GSE62165, GSE71729) consistently confirmed elevated CD58 expression in PDAC tissues compared with both ANCTs and normal pancreatic tissues (figure 1C–F). Given that PDAC arises through a progressive, multistep process from precursor lesions,[36] we examined CD58 expression in low-grade pancreatic lesions using the GSE19650 dataset. The analysis revealed that CD58 transcript levels were higher in intraductal papillary mucinous neoplasm tissues than in normal pancreatic tissues (figure 1G), suggesting that its upregulation may be an early event in PDAC tumorigenesis. To explore the relationship between CD58 expression and cancer stem cell (CSC) properties, we analyzed the GSE51971 dataset after stratifying samples by CSC marker (CD44/CD133/EpCAM). Notably, CD58 expression was elevated in the triple-positive group (figure 1H), indicating its potential role in PDAC stemness (figure 1H). UALCAN database showed that CD58 expression correlated with tumor differentiation, exhibiting higher levels in poorly differentiated PDAC (figure 1I). Additionally, CD58 expression was significantly increased in PDAC tissues from patients harboring TP53 mutations (figure 1J), a genetic alteration commonly associated with tumor aggressiveness and poor prognosis. Survival analysis using the LinkedOmics platform illustrated that patients with high CD58 expression had a shorter median survival (17.0 months) compared with those with low expression (37.7 months; n=86 per group, p<0.001) (figure 1K), identifying CD58 as a predictor of poor prognosis.

To validate these findings, we established a spontaneous PDAC model using orthotopic pancreatic implantation of the potent carcinogen DMBA in C57BL/6 mice. Successful induction of PDAC was confirmed by HE staining (figure 1L). IHC analysis showed stronger CD58 staining in PDAC tissues compared with murine normal pancreatic tissues and ANCTs (figure 1L). Moreover, IF analysis revealed increased CD58 fluorescence intensity in PDAC tissues relative to matched ANCTs (figure 1M). Collectively, these findings provide robust evidence that CD58 is upregulated in PDAC and precursor lesions, correlates with cancer stemness, poor differentiation, TP53 mutations, and worse prognosis. These data reinforce our previous findings[34] and suggest that CD58 may serve as a novel prognostic biomarker for PDAC.

Subcellular localization of CD58 molecules and functional effects on PDAC cells

To investigate the subcellular localization of CD58 in PDAC, we performed IHC and IF staining on human PDAC tissues. The results revealed that CD58 was primarily membrane-localized but also detected in the cytoplasm. Notably, in a subset of PDAC cells, CD58 exhibited prominent cytoplasmic accumulation, forming distinct "cytoplasmic pools" (figure 2A). To further delineate the intracellular distribution of CD58, confocal IF imaging was conducted using two PDAC cell lines, Panc-1 and AsPC-1. AsPC-1 showed predominant membrane localization, whereas Panc-1 displayed both membrane and cytoplasmic distribution (figure 2B), indicating potential cell line-dependent variation in subcellular localization.

Next, we assessed CD58 expression levels across a panel of PDAC cell lines. Compared with HPNE controls, CD58 was significantly upregulated at both the mRNA and protein levels in AsPC-1, BxPC-3, SW1990, and CFPAC-1 cells (figure 2C,D). Panc-1 cells showed elevated CD58 protein but not mRNA levels. Based on these findings, Panc-1 cells (low-CD58) and AsPC-1 cells (high-CD58) were selected for functional studies. Stable CD58 knockdown was successfully established in both lines (figure 2E, online supplemental Figure 1C). Surprisingly, CD58 knockdown showed no significant effect on cell viability, proliferation, migration, or invasion in vitro (online supplemental Figure 1D–G). This observation was further corroborated by in vivo studies using NSG immunodeficient mice, where CD58 depletion did not affect tumor growth and metastasis in cell-derived xenografts and pulmonary metastasis models (online supplemental Figure 1H–M). These findings suggest that although CD58 is upregulated and differentially localized in PDAC, its role in regulating these

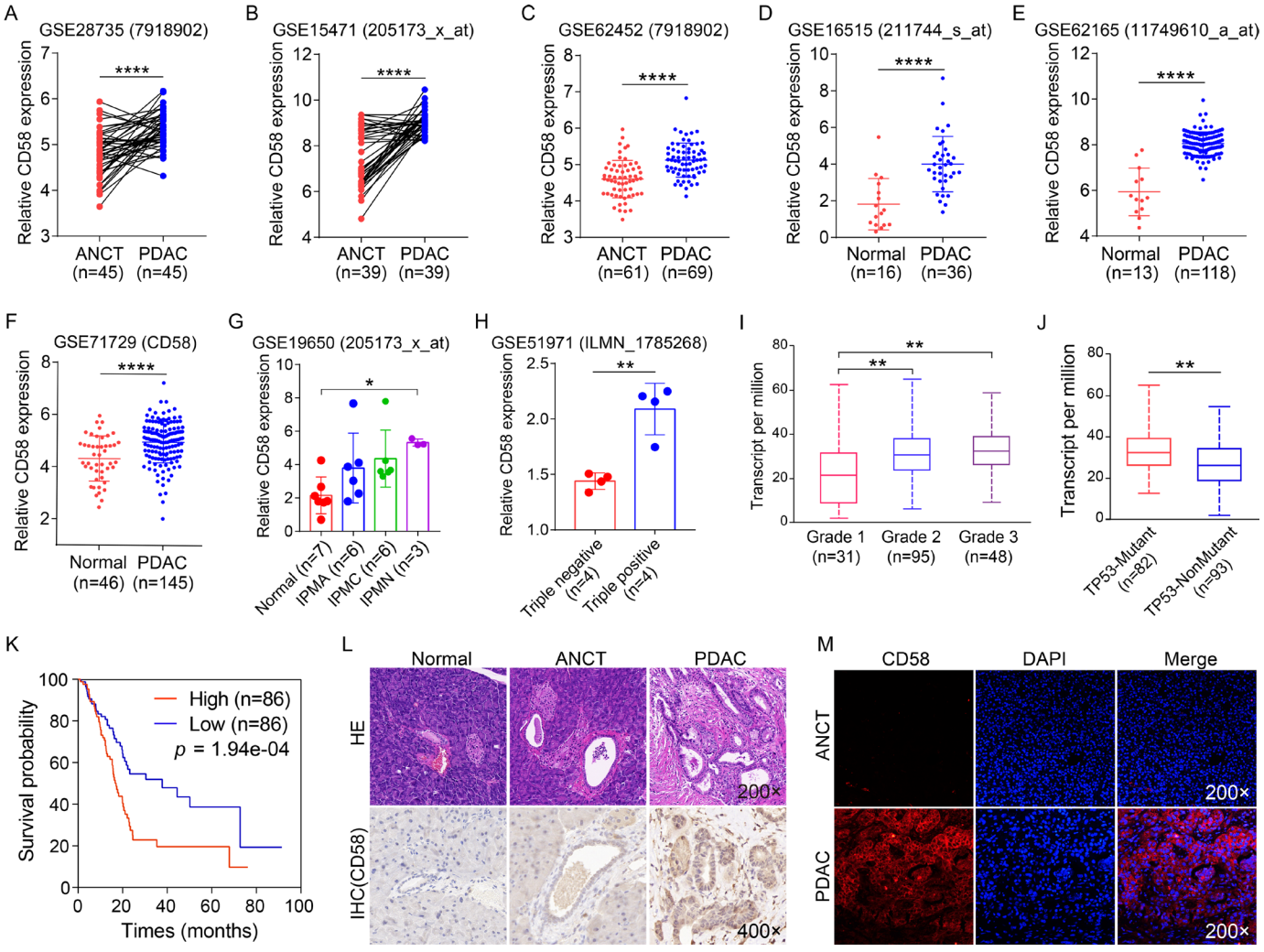

Figure 1 CD58 is elevated in PDAC tissues and acts as an adverse prognostic predictor. (A, B) GSE28735 (45 pairs) and GSE15471 (39 pairs) data subsets. (C–F) GSE62452 (61 vs 69), GSE16515 (16 vs 36), GSE62165 (13 vs 118) and GSE71729 (46 vs 145) data subsets. (G) The GSE19650 contains normal pancreatic tissue (n=7), IPMA (n=6), IPMC (n=6), and IPMN (n=3). (H) The GSE51971 was divided into triple-negative (n=4) and triple-positive (n=4) groups according to three cancer stem cell markers, CD44, CD133, and EpCAM. Following the GSE data subset, the probe name of the CD58 used is in parentheses. (I) UALCAN platform for PDAC differentiation analysis (31 vs 95 vs 48). (J) Analysis of CD58 expression in patients with or without TP53 mutations (82 vs 93) from UALCAN. (K) LinkedOmics platform was used to analyze the survival prognosis of PDAC patients with high and low CD58 expression (86 vs 86, p=1.94e–4). (L) HE and IHC staining of normal pancreatic tissue, ANCT and PDAC tissue in mice. (M) IF staining of human PDAC tissue with CD58 in red and DAPI (nucleus) in blue. Mean±SD, *p<0.05, **p<0.01, ****p<0.0001. ANCT, adjacent non-cancerous tissues; IF, immunofluorescence; IHC, immunohistochemical; IPMA, intraductal papillary mucinous adenoma; IPMC, intraductal papillary mucinous carcinoma; IPMN, intraductal papillary mucinous neoplasm; PDAC, pancreatic ductal adenocarcinoma; UALCAN,University of Alabama at Birmingham CANcer data analysis Portal.

canonical tumor cell behaviors may be limited or context-dependent.

PDAC-induced transformation of immature macrophages to M2-like type

THP-1 monocytes were differentiated into primitive M0 macrophages by treatment with PMA, leading to cellular adherence and morphological changes consistent with macrophage differentiation (figure 2F). To assess PDAC-induced macrophage polarization, we established an indirect co-culture system using transwell inserts with a 0.4 µm pore size, allowing for the exchange of soluble factors while preventing direct cell-cell contact (figure 2I). Following co-culture with PDAC cells, M0 macrophages acquired the phenotypic features of TAMs, characterized by decreased M1 markers (IFN-γ and iNOS) and increased M2 markers (CD163, Arg-1, and TGF-β) (figure 2G,H). Flow cytometry further verified increased expression of M2 surface markers CD163 and CD206 on TAMs (figure 2J,K), supporting the induction of an M2-like immunosuppressive phenotype.

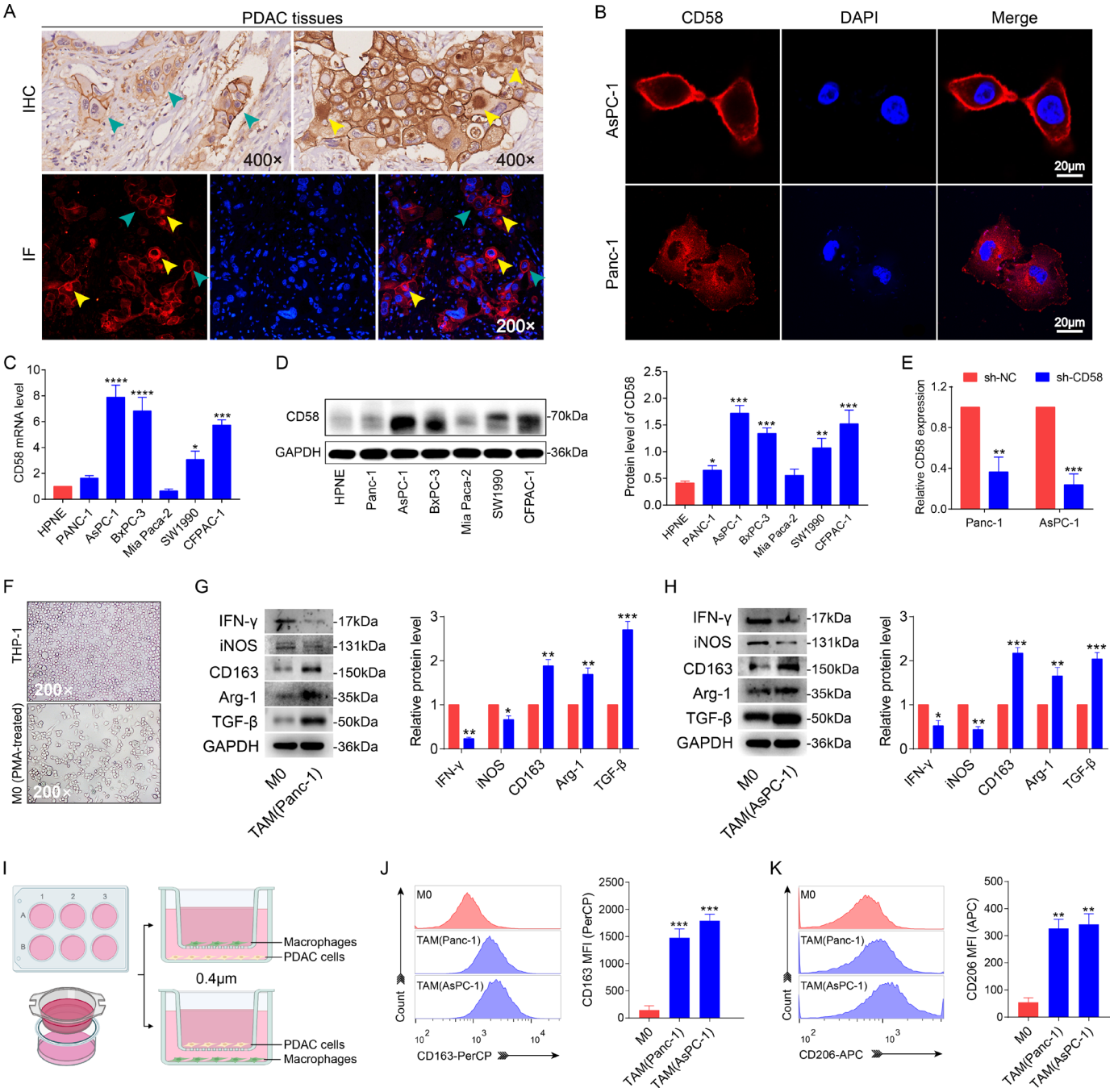

Figure 2 Subcellular localization of CD58 molecules and PDAC-induced transformation of immature macrophages. (A) IHC and IF staining of CD58 in PDAC tissues. CD58 is red fluorescent and DAPI is blue fluorescent. Green arrows refer to CD58 located in the membrane, and yellow arrows refer to CD58 located in the cytoplasm and "cytosolic pool". Magnification is shown. (B) CD58 confocal imaging in PDAC cell lines. CD58 is red fluorescent and DAPI is blue fluorescent. White bar, 20 μm. (C, D) Expression of CD58 mRNA and protein in various PDAC cell lines. (E) CD58 knockdown was validated by qRT-PCR. (F) Monocyte THP-1 was induced as primary macrophage M0 by PMA at a final concentration of 100 ng/mL. Magnification: 200×. (G, H) After co-culture, the expression of M1 and M2 markers in TAM was detected by Western blotting. (I) Co-culture diagram of immature macrophages M0 and PDAC cells, 0.4 μm pore size. (J, K) Flow cytometry was used to detect M2 markers, CD163 and CD206, on the surface of TAMs. Mean±SD, *p<0.05, **p<0.01, ***p<0.001, ****p<0.0001. IF, immunofluorescence; IHC, immunohistochemical; PDAC, pancreatic ductal adenocarcinoma; qRT-PCR, quantitative real-time PCR; TAMs, tumor-associated macrophages.

Expression of CD58 is associated with the TGF-β/Smad2/3 pathway

Given that TGF-β was the most markedly upregulated factor in PDAC-educated macrophages, we next explored this signaling pathway. Using the GEPIA and TIMER databases, we found a positive correlation between CD58 and TGF-β/Smad2/3 signaling pathway (figure 3A,B). RT-PCR analysis of seven PDAC cell lines warranted a

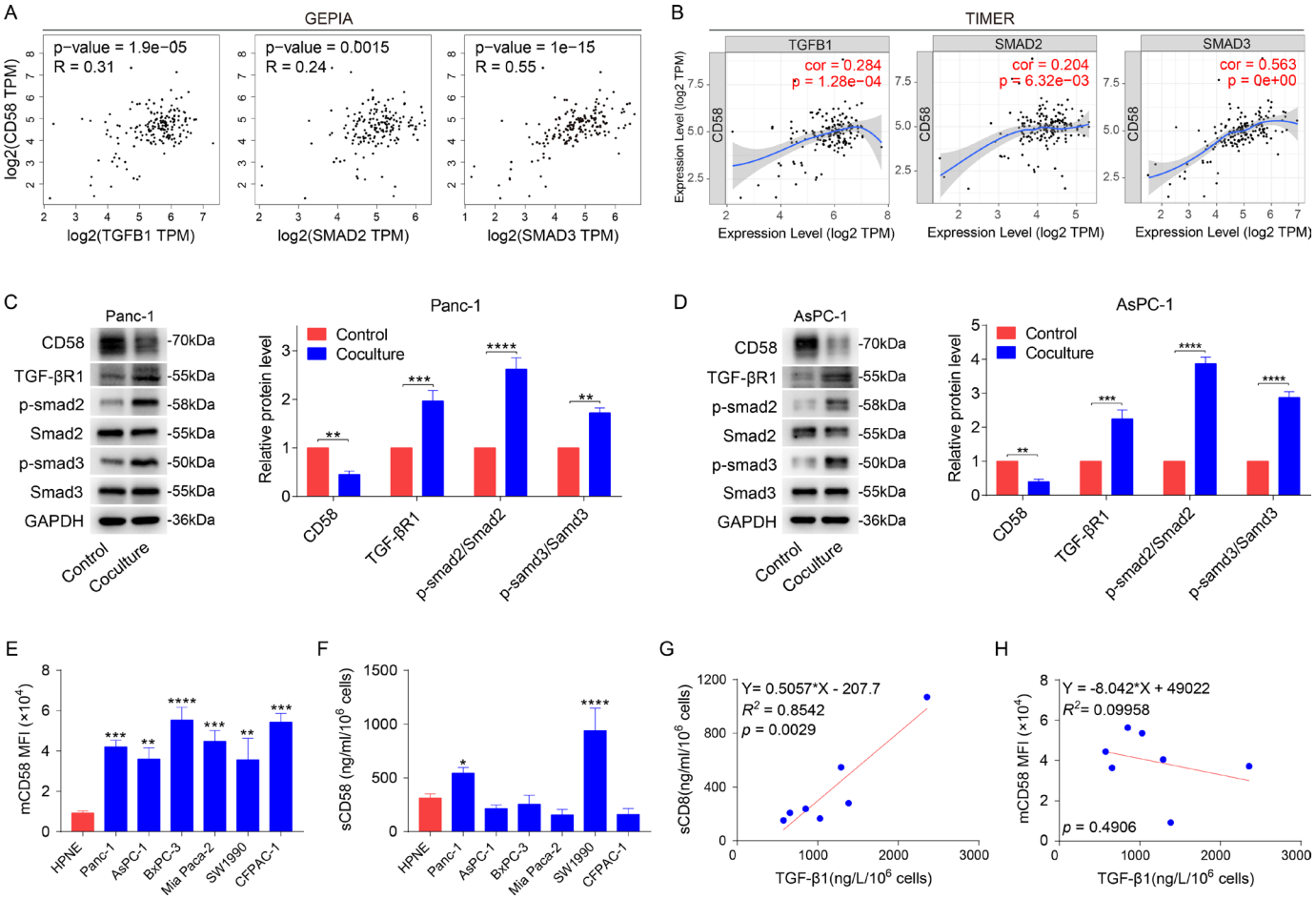

Figure 3 Expression of CD58 is significantly associated with the TGF-β/smad2/3 pathway. (A, B) Correlation module in GEPIA (n=179) and TIMER (n=178) databases of online bioinformatics platforms on the transcription levels of CD58 and TGF-β/smad2/3 pathway-related genes (Spearman correlation). (C, D) Western blot was used to detect the protein expression of TGF-β/smad2/3 pathway and CD58 in PDAC cells after co-culture. (E) Flow cytometry was used to detect the expression level of mCD58 on the surface of PDAC cells. (F) ELISA was used to detect the content of sCD58 in the supernatant of PDAC cells (ng/mL/10^6 cells). (G) The correlation between TGF-β1 (ng/mL/10^6 cells) and sCD58 (ng/mL/10^6 cells) contents in the supernatant of PDAC cells (Pearson correlation, p=0.0029). (H) The correlation between TGF-β1 (ng/mL/10^6 cells) and cell surface mCD58 expression (MFI) in the supernatant of PDAC cells (Pearson correlation, p=0.4906). Mean±SD, *p<0.05, **p<0.01, ***p<0.001, ****p<0.0001. MFI, mean fluorescence intensity; PDAC, pancreatic ductal adenocarcinoma; GEPIA,Gene Expression Profiling Interactive Analysis ; TIMER, Tumor Immune Estimation Resource.

significant positive correlation between TGF-β1 and CD58 mRNA levels (online supplemental Figure 2A). Unexpectedly, following 72 hours of indirect co-culture, we observed activation of the TGF-β/Smad2/3 pathway accompanied by decreased CD58 protein level (figure 3C–D). This finding seems to be contrary to the positive correlation mentioned above. In fact, beyond membrane-bound CD58 (mCD58), a soluble form also exists (sCD58).[31] Next, we examined the mean fluorescence intensity of mCD58 on the surface of PDAC cell membranes by flow cytometry and the content of sCD58 in the culture supernatant by ELISA. Compared with HPNE, mCD58 was increased in multiple PDAC cell lines (figure 3E), while sCD58 was only elevated in the supernatant of Panc-1 and SW1990 cells (figure 3F). Although sCD58 was not elevated in all PDAC cell supernatants, a significant positive correlation was identified between sCD58 and TGF-β1 (figure 3G). However, no significant correlation was observed between mCD58 and TGF-β1 in the supernatant (figure 3H).

TGF-β1 promotes the expressional separation of CD58 by Smad2/3 signaling pathway

To investigate the impact of TAMs on CD58 expression in PDAC cells, we examined both mCD58 and sCD58 in the context of indirect co-culture. Flow cytometry showed a reduction in mCD58 expression on the surface of PDAC cells following co-culture with TAMs (figure 4A,B), whereas ELISA revealed a concomitant increase in supernatant sCD58 (figure 4C). This inverse pattern—characterized by decreased membrane expression and increased soluble production—was here referred to as “expressional separation”. To elucidate the regulatory mechanism underlying this phenomenon, we modulated the TGF-β/Smad2/3 signaling pathway, a crucial immunomodulatory axis in the TME. Specifically,

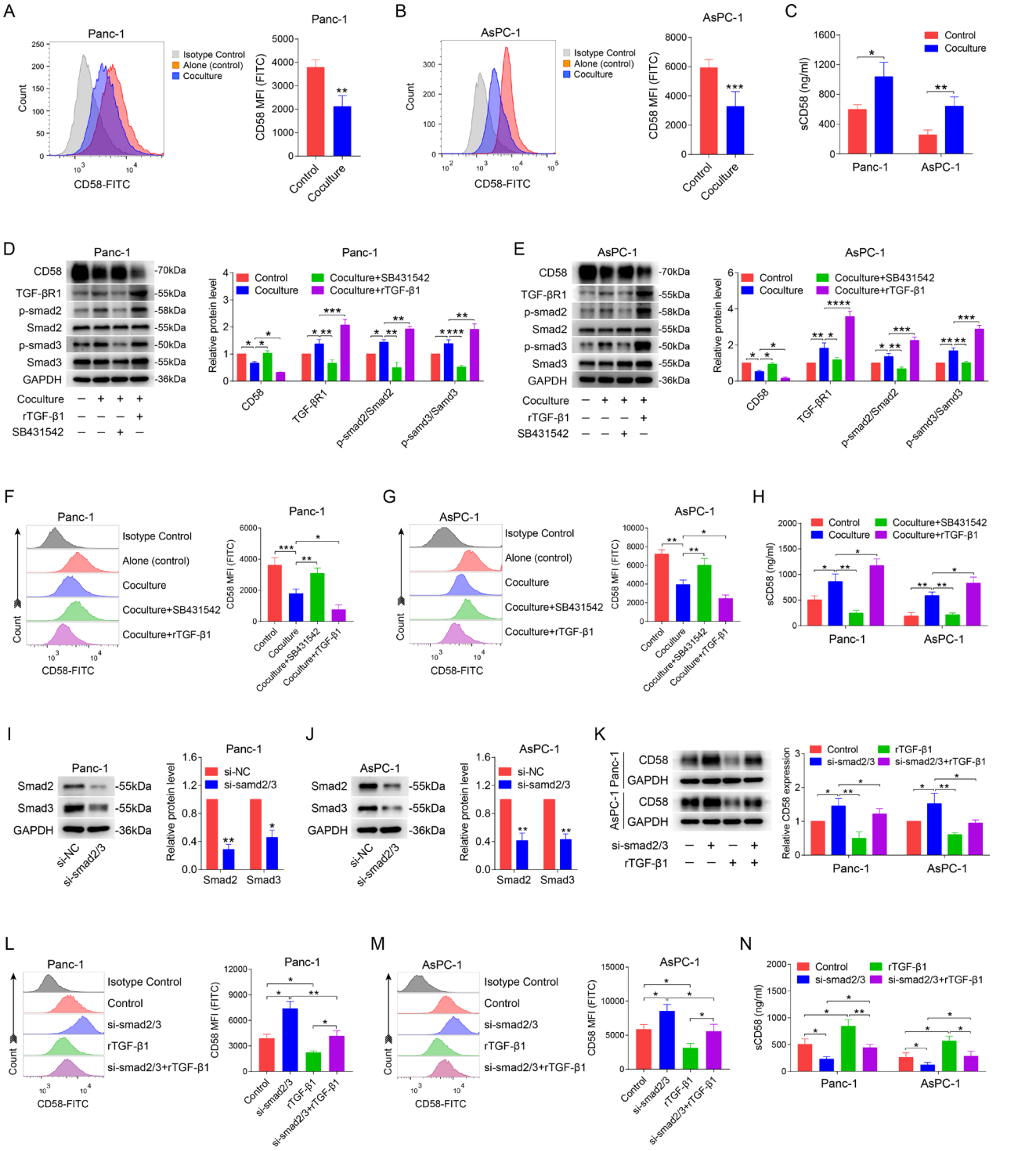

Figure 4 TGF-β1 promotes the expressional separation of CD58 by Smad2/3 signaling pathway. (A, B) Expression of mCD58 on the surface of PDAC cells after co-culture was detected by flow cytometry. (C) ELISA was used to detect the content of sCD58 (ng/mL) in the culture medium after co-culture. (D, E) Western blot was used to detect the protein expression of CD58 after stimulation and blockade of TGF-β/smad2/3 pathway by rTGF-β1 and SB431542, respectively. (F, G) Flow cytometry was used to detect mCD58 expression (MFI) on the cell membrane surface of PDAC cells after stimulation and blockade of TGF-β/smad2/3 pathway by rTGF-β1 and SB431542, respectively. (H) ELISA was used to detect the content of sCD58 (ng/mL) in the culture supernatant after rTGF-β1 and SB431542 stimulated and blocked TGF-β/smad2/3 signaling pathway, respectively. (I, J) Western blot was used to verify the knockdown effect of smad2/3. (K) The protein expression of CD58 in PDAC cells in response to si-smad2/3, rTGF-β1 and their combination. (L, M) Flow cytometry was used to detect the expression of mCD58 on the surface of PDAC cells exposed to si-smad2/3, rTGF-β1, and their combination factors (MFI). (N) ELISA was used to detect the content of sCD58 (ng/mL) in the supernatant of PDAC cells in response to si-smad2/3, rTGF-β1, and their combined factors. Mean±SD, *p<0.05, **p<0.01, ***p<0.001, ****p<0.0001. MFI, mean fluorescence intensity; NC, normal control; PDAC, pancreatic ductal adenocarcinoma.

recombinant human TGF-β1 (rTGF-β1) was used to activate the pathway, while SB431542, a selective inhibitor of TGF-β type I receptor kinase, was employed to block it (figure 4D,E). SB431542-mediated TGF-β/Smad2/3 inhibition increased mCD58 expression while reducing supernatant sCD58 (figure 4F–H), suppressing the expressional separation of CD58. Conversely, rTGF-β1 stimulation diminished mCD58 but elevated sCD58 (figure 4F–H), effectively enhancing the expressional separation. To further confirm that the observed effects were mediated via the Smad2/3 signaling cascade, we performed siRNA-mediated knockdown (figure 4I,J). Silencing of Smad2/3 elevated mCD58 and reduced sCD58 production (figure 4K–N), indicating the attenuation of expressional separation. Furthermore, Smad2/3 knockdown could effectively reverse the rTGF-β1-induced expressional separation (figure 4K–N), further confirming the regulatory role of this pathway.

sCD58 fails to induce M0 polarization to M2 type in naive macrophages

To determine whether sCD58 supernatant could drive M0-to-M2 macrophage polarization in the co-culture system, we designed a series of concentration gradients of active recombinant human CD58 protein (rCD58) to induce naive macrophage M0, M2 markers on the macrophage surface were detected. FCM demonstrated that CD163 and CD206 on the macrophage surface were not significantly changed in each group (online supplemental Figure 2B and C). Moreover, there were no significant statistical differences in the TGF-β1 content in the supernatant between the groups (online supplemental Figure 2D). These results suggested that sCD58 does not induce polarization of M0 in naive macrophages toward the M2 type.

The expressional separation of CD58 inhibits T cell cytotoxicity in vitro

Although CD58 is widely distributed in human cells and tissues, the CD58 gene has not been identified in mice. The only counter receptor for CD2 identified to date is CD48.[37] Because of its highly similar distribution and structure, murine CD48 is considered a homologous gene for human CD58.[38 39] To keep the full-text names consistent and avoid confusion, murine CD48 was collectively called cd58 in the following text. Murine PDAC cell lines (Panc02s and KPC) with stable cd58 overexpression were obtained via lentiviral lv-cd58 transfection and puromycin selection (online supplemental Figure 2E and F). Colony formation and CCK-8 assays showed that cd58 has no effect on the survival activity and proliferation in murine PDAC cells (online supplemental Figure 2G–I).

Subsequently, we hypothesized that sCD58 may act as a decoy molecule by competitively binding to CD2 on T/NK cells, thereby impairing immune recognition of tumor cells via disrupting CD2-CD58 axis. We isolated $CD3^+$ $CD8^+$ T cells and $CD3^-$ $NKp46^+$ NK cells from spleens of C57BL/6 mice using T/NK cell isolation kits. Flow cytometry was used to analyze CD2 expression in T/NK cells, and the gating strategy is shown in online supplemental Figure 3A). The positive rate of CD2 on the surface of T/NK cells was nearly 100% (online supplemental Figure 3B and C).

To investigate the effect of sCD58 on T cell cytotoxicity in vitro, C57BL/6 mice received 3 weekly abdominal injections of heat-inactivated (60°C) Panc02 or KPC cells to generate PDAC-specific memory. Mouse splenic T cells were extracted and activated by CD3/CD28 beads combined with IL-2 stimulation. Activated cytotoxic T lymphocytes (CTLs) were directly co-cultured with Panc02 or KPC for 24 hours, and then T cell cytotoxicity and activation were detected. It was easy to separate the two using the characteristics of PDAC cells adhering while T cells grew in suspension. GFP^- $CD8^+$ T cell populations were obtained by a specific gating strategy (online supplemental Figure 3D). Direct co-culture revealed T cell-mediated killing of Panc02 or KPC cells, evidenced by the clustering of CTLs around apoptotic tumor cells (figure 5A). Recombinant murine cd58 (rm-cd58) mimicking sCD58 was added to co-culture dishes between CTLs and PDAC cells to observe the effect of rm-cd58 on CTL cytotoxicity. The LDH release assays demonstrated that PDAC cells overexpressing cd58 exhibited enhanced susceptibility to CTL-mediated killing, while the addition of rm-cd58 attenuated CTL cytotoxicity (figure 5B). CD107a and Perforin were directly related to CTL cytotoxic activity. The flow cytometry results showed that cd58 augmented the levels of CD107a and Perforin, whereas rm-cd58 successfully suppressed the expression of CD107a and Perforin in CTLs (figure 5C,D). Besides, blockade of CD2 with mAbs abolished the inhibitory effect of rm-cd58 on CTL cytotoxicity, indicating rm-cd58 functions by competing with anti-CD2 mAb for CD2 binding (online supplemental Figure 3E). Altogether, these findings suggested that sCD58 interferes with adhesion recognition of PDAC cells by T cells via disrupting the CD2-CD58 axis, thereby alleviating immune killing of PDAC cells by CTLs.

mCD58 facilitates and sCD58 dampens T/NK cell cytotoxicity in murine subcutaneous tumor-bearing models

Mice were regularly monitored weekly for changes in body weight and tumor volume. No significant differences in body weight were observed between the groups during the 4-week monitoring period (figure 6A and E), while significant differences in tumor volume were detected (figure 6B and F). Compared with the NC group, tumor volume in the cd58-overexpressing group was smaller. Tumor volume in the lv-cd58 combined with rm-cd58 was larger than that in lv-cd58 group (figure 6C and G). Similarly, subcutaneous tumor weight was lighter in the cd58-overexpressing group than in controls, while the lv-cd58+rm-cd58 group exhibited heavier tumor weight compared with lv-cd58 alone (figure 6D and H).

Next, we assessed the activation status of infiltrating T/NK cells within the tumor mass using flow cytometry.

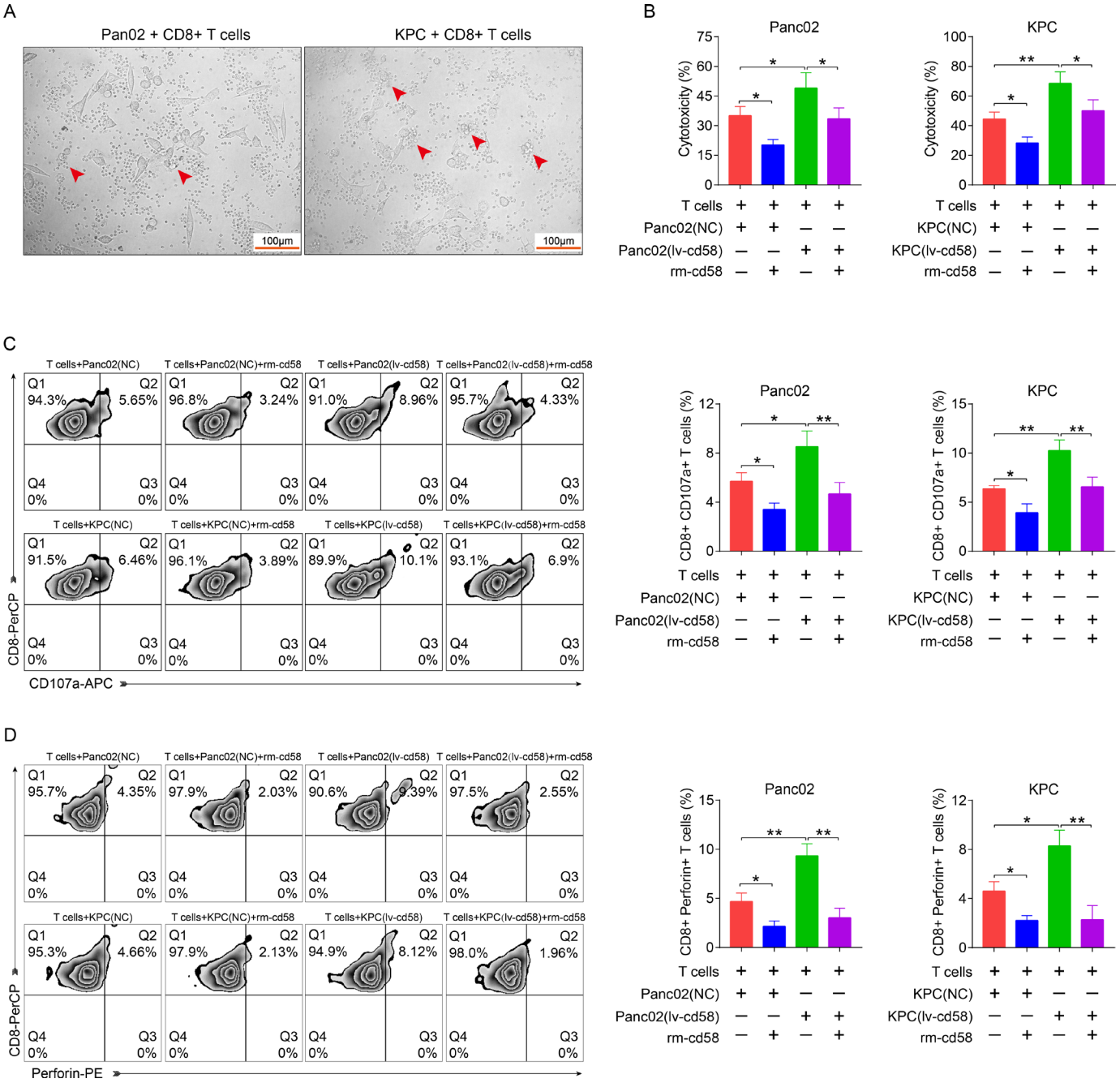

Figure 5 The expressional separation of CD58 inhibits T cell cytotoxicity in vitro. (A) The immune killing of PDAC cells by CTLs was observed under light microscope (10:1). Red arrows point to apoptotic PDAC cells. Red bar, 100 μm. (B) LDH release assays were utilized to assess the CTL cytotoxicity. (C, D) The proportion of CD107a and Perforin in CTLs in different experimental groups. Mean±SD, *p<0.05, **p<0.01. CTLs, cytotoxic T lymphocytes; lv-cd58, lentivirus-transfected cd58; LDH, lactate dehydrogenase; NC, normal control; PDAC, pancreatic ductal adenocarcinoma; rm-cd58, recombinant murine cd58.

Activated NK cells were defined as $CD45^+$ $CD3^-$ $CD49b^+$ $CD107a^+$ or $CD45^+$ $CD3^-$ $CD49b^+$ $NKG2D^+$; activated CTLs were $CD45^+$ $CD3^+$ $CD8^+$ $CD107a^+$ or $CD45^+$ $CD3^+$ $CD8^+$ $Perforin^+$. The gating strategy is shown in online supplemental Figure 4. For infiltrating NK cells, the proportion of $CD107a^+$ and $NKG2D^+$ NK cells in the lv-cd58 group was higher than that in controls, while the proportion of $CD107a^+$ and $NKG2D^+$ NK cells diminished after combined rm-cd58 (figure 6I,J, online supplemental Figure 5A and B). Similarly, for infiltrating CTLs, the proportion of $CD107a^+$ and $Perforin^+$ CTLs was higher in the lv-cd58 group than in controls, whereas the proportion of $CD107a^+$ and $Perforin^+$ CTLs was reduced after combined rm-cd58 (figure 6K,L, online supplemental Figure 5C and D). The IF staining of CD206 revealed substantial infiltration of M2-like macrophages in PDAC tissues. Tumor size is correlated with the abundance of M2-like macrophages in the TME (online supplemental Figure 6A). An additional set of cell-derived xenograft models illustrated that stimulation with TGF-β1

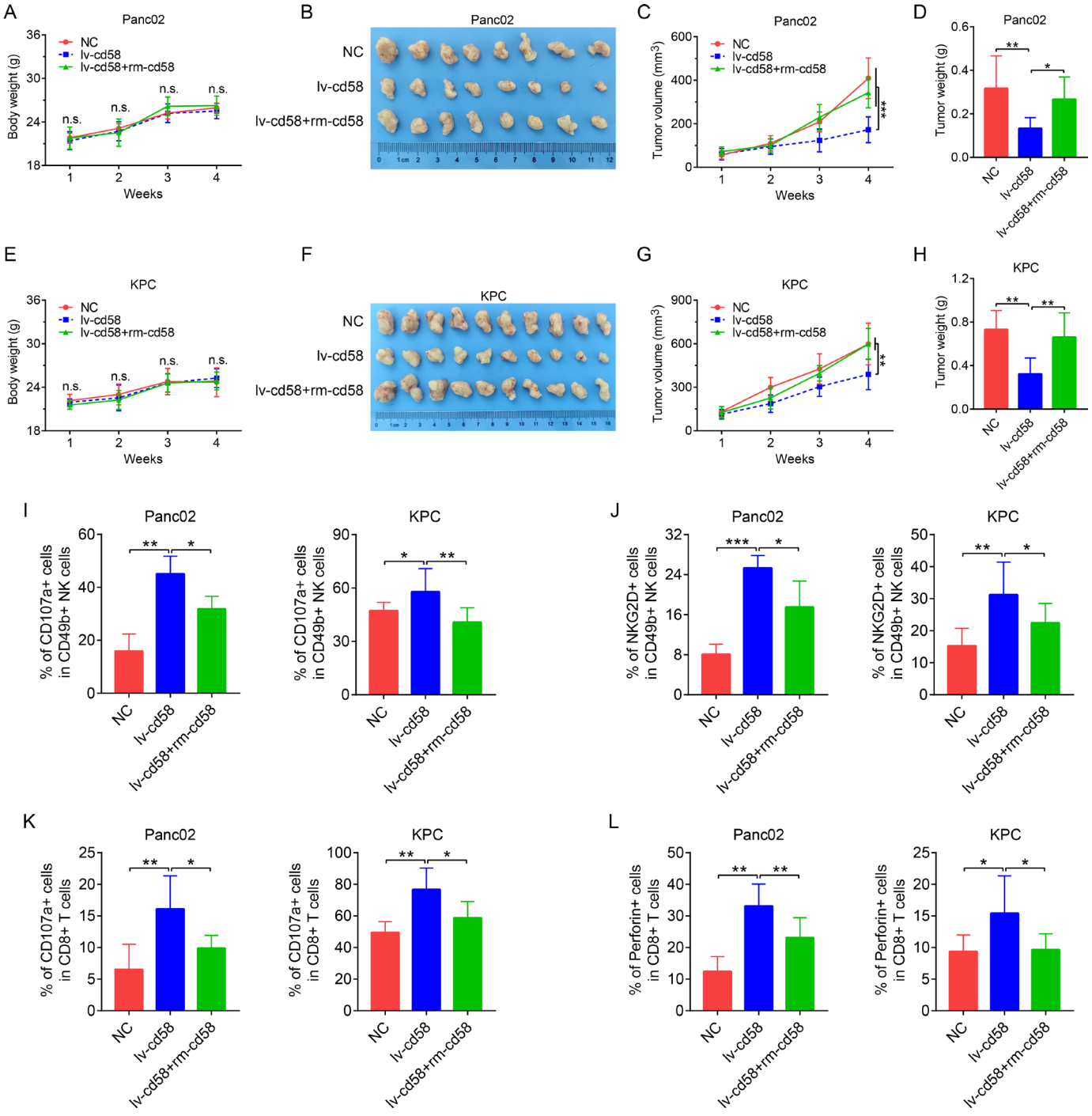

Figure 6 The mCD58 facilitates and sCD58 dampens T/NK cell cytotoxicity in subcutaneous tumor-bearing models. (A, E) Body weight monitoring in immunocompetent C57BL/6 mice (g). (B, F) Photographs of subcutaneous tumors in each group were taken. Of these, the lv-cd58+rm-cd58 group was injected with 100 µL of rm-cd58 at a concentration of 5 mg/mL around the tumor mass twice a week. 4 weeks later, mice were sacrificed and subcutaneous tumors were weighed and photographed. Panc02, 8 mice per group; KPC, 10 mice per group. (C, G) Subcutaneous tumor volume monitoring. The length and short diameter of the subcutaneous tumor mass in mice were measured using a vernier caliper, and the volume (mm^3) was calculated. (D, H) Comparison of subcutaneous tumor weight in mice (g). (I, J) The proportion of $CD107a^+$ and $NKG2D^+$ in infiltrating NK cells in the tumor mass between the groups. (K, L) The proportion of $CD107a^+$ and $Perforin^+$ in infiltrating CTLs between the groups. Flow staining labeled fluorescence: CD49b-PE, CD107a-BV510, NKG2D-APC, CD8-PerCP/Cy5.5, Perforin-PE. Mean±SD, n.s., not significant. *p<0.05, **p<0.01, ***p<0.001. lv-cd58, lentivirus-transfected cd58; NC, normal control; rm-cd58, recombinant murine cd58.

accelerated tumor growth by enhancing the expressional separation of CD58, while overexpression of mCD58 at least partially reversed this process (online supplemental Figure 6B–D). Taken together, these findings suggested that mCD58 overexpression enhances T/NK cell-mediated immune killing of PDAC cells via CD2-CD58 interactions. In contrast, high local concentrations of sCD58 interfere with immune recognition by disrupting the CD2-CD58 axis, thereby reducing T/NK cell activation. TGF-β1 promotes T/NK cell-mediated immune escape by the expressional separation of CD58 in PDAC.

In addition, the positivity rate of cd58 in PDAC cells was detected using flow cytometry after digesting the tumor mass into single cells with collagenase. Unexpectedly, although the positive rate of cd58 in the lv-cd58 and lv-cd58+rm-cd58 groups remained higher than that in controls (online supplemental Figure 6E and F), it showed a significant decrease compared with preinoculation levels (online supplemental Figure 6G). Interestingly, the positive rate of cd58 was higher in the lv-cd58+rm-cd58 group than in the lv-cd58 group (online supplemental Figure 6E–G). HE and IHC staining of the subcutaneous tumor were performed (online supplemental Figure 6H and I), confirming the above findings. This is likely associated with the preferential killing of CD58-high-expressing cells by T/NK cells within the polyclonal cell population.

The expressional separation of CD58 suppresses T/NK cell-mediated immune killing in intraperitoneal dissemination models

Intraperitoneal dissemination models in immunocompetent mice were established by intraperitoneal injection of PDAC cell suspensions. PDAC cells successfully formed multiple metastases and spread in the abdominal cavity of mice, mainly concentrated in the mesentery, bilateral inguinal regions, and around the hepatogastric region (figure 7A). Compared with the NC group, peritoneal dissemination of PDAC cells was strikingly ameliorated in the lv-cd58 group, but this reduction was abrogated by rm-cd58 co-administration (figure 7A). Mice maintained a stable body weight with no significant differences between groups (online supplemental Figure 7A). Flow analysis of peritoneal lavage fluid manifested that the injection of PDAC cell suspensions increased the proportion of $CD3^+$ lymphocyte infiltration. The abundance of lymphocytes was further enhanced after overexpression of cd58 (lv-cd58 group), while rm-cd58 co-treatment attenuated this effect (online supplemental Figure 7B).

Next, we evaluated the activation of infiltrating T/NK cells in the peritoneal cavity of mice. For NK cells, the NC group successfully increased the proportion of $CD107a^+$ and $NKG2D^+$ NK cells. This proportion of activated NK cells was further augmented after overexpression of cd58, while the proportion of activated NK cells infiltrated in the peritoneal cavity of mice was decreased after using rm-cd58 (figure 7B–C, online supplemental Figure 7C and D). Analogously, for CTLs, NC group effectively increased the proportion of $CD107a^+$ and $Perforin^+$ CTLs. Overexpression of cd58 further enhanced CTL activation, whereas rm-cd58 treatment diminished peritoneal infiltration of activated CTLs (figure 7D,E, online supplemental Figure 7E and F). Moreover, immune inflammatory cytokines IFN-γ, TNF-α, and TGF-β1 in peritoneal lavage fluid of mice were detected. IFN-γ and TNF-α in the NC group were elevated compared with those in the PBS group (figure 7F,G). The levels of IFN-γ and TNF-α in the peritoneal cavity of mice were further increased after overexpression of cd58, while rm-cd58 effectively curtailed the contents of IFN-γ and TNF-α (figure 7F,G). As expected, TGF-β1 levels showed a positive correlation with the severity of intraperitoneal dissemination, further confirming that TGF-β1 facilitated PDAC malignant progression by the expressional separation of CD58 (online supplemental Figure 7G). The more severe the inflammatory reaction in the abdominal cavity, the more inflammatory cells accumulate in the spleen. Therefore, spleen weight could reflect the inflammatory state of the abdominal cavity to some extent. Compared with the PBS group, spleen weight was higher in the NC group and further increased with cd58 overexpression (lv-cd58). Of note, rm-cd58 co-administration attenuated this effect (online supplemental Figure 7H). Altogether, these results confirmed the aforementioned hypothesis.

Prognostic significance and diagnostic value of circulating sCD58 in PDAC patients

Combined with the above findings, we speculate that high concentrations of sCD58 accumulated in tumor tissue are likely released into the blood via neovascularization in the TME. Subsequently, 303 serum samples were obtained from participants, including 171 PDAC patients and 132 healthy controls. The levels of sCD58 and TGF-β1 in the serum of PDAC patients were higher than those of the healthy controls (figure 8A,B). To investigate whether serum levels of sCD58 and TGF-β1 are elevated early in PDAC, we compared stage I/II patients with healthy controls. Serum sCD58 levels showed no significant difference between stage I patients and controls but were elevated in stage II (online supplemental Figure 8A). In contrast, TGF-β1 levels were already increased in stage I and remained enhanced in stage II (online supplemental Figure 8B). The scatter plot exhibited a significant positive correlation between serum sCD58 and TGF-β1 levels in PDAC patients (n=171, p=0.0059, figure 8C). Through analyzing the correlation between serum sCD58 and clinicopathological characteristics of PDAC patients, it was found that the serum sCD58 level was strongly correlated with tumor size (p=0.026), distant metastasis (p=0.043), TNM stage (p=0.011) and macrovascular invasion (p=0.025) (table 1, online supplemental Figure 8C–F). Serum TGF-β1 level in PDAC patients was significantly associated with perineural invasion (p=0.0003, online supplemental Table S4).

To evaluate the diagnostic potential of sCD58 and TGF-β1 for PDAC, additional sera were collected from 213 patients with benign pancreatic disease. Therefore, a total

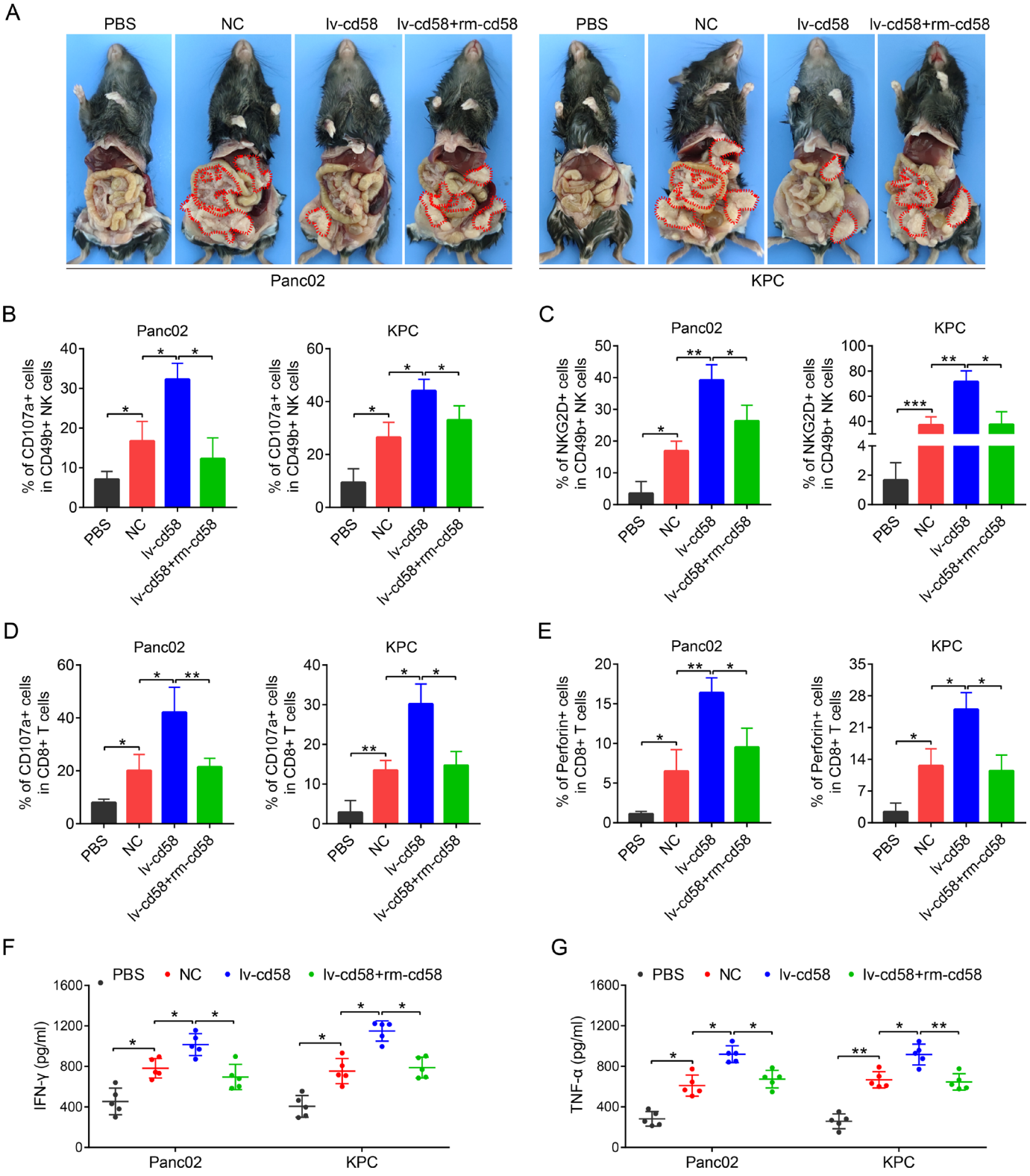

Figure 7 The expressional separation of CD58 suppresses T/NK cell-mediated immune killing in intraperitoneal dissemination models. (A) Establishment of intraperitoneal xenograft model in mice. Typical diagram, five mice in each group. Red circles represent areas of disseminated tumor seeding. (B, C) The proportion of $CD107a^+$ and $NKG2D^+$ in NK cells between the groups. (D, E) The proportion of $CD107a^+$ and $Perforin^+$ in CTLs between the groups. Flow staining labeled fluorescence: CD49b-PE, CD107a-BV510, NKG2D-APC, CD8-PerCP/Cy5.5, Perforin-PE. (F, G) The contents of IFN-γ and TNF-α in the peritoneal lavage fluid of mice in each group, respectively. Mean±SD, n.s., not significant. *p<0.05, **p<0.01, ***p<0.001. lv-cd58, lentivirus-transfected cd58; NC, normal control; rm-cd58, recombinant murine cd58; PBS, phosphate buffered saline.

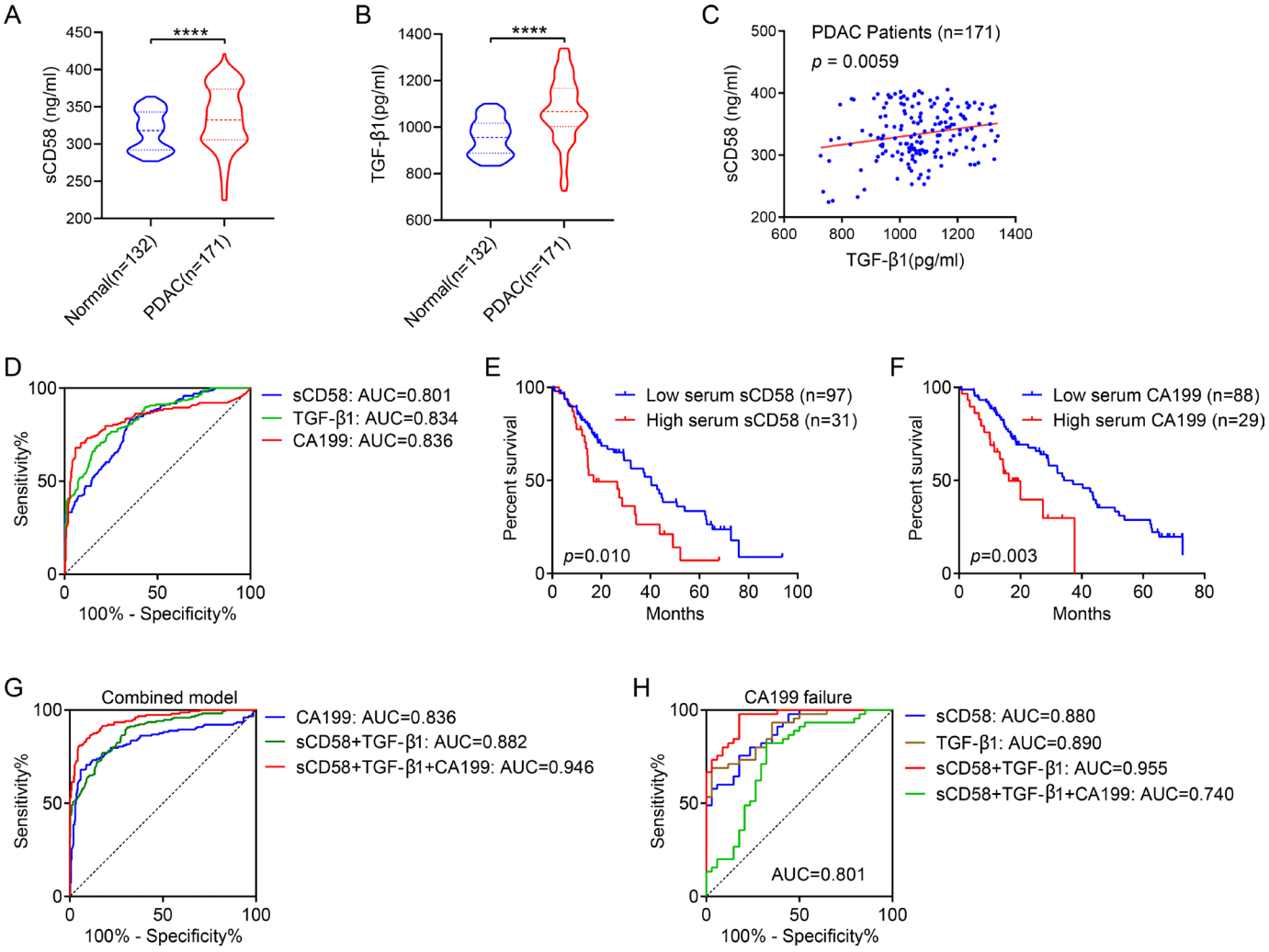

Figure 8 Prognostic significance and diagnostic value of serum sCD58 in PDAC patients. (A, B) Serum levels of sCD58 and TGF-β1 in patients with PDAC (Mann-Whitney *U* test). (C) Scatterplot and correlation analysis of sCD58 and TGF-β1 in serum of PDAC patients (n=171) (Pearson correlation, p=0.0059). (D) ROC curves for sCD58, TGF-β1, CA199 as diagnostic markers. (E, F) Higher serum levels of sCD58 and CA199 predicted shorter overall survival in patients with PDAC (p=0.010, p=0.003, respectively). (G) ROC curves for dual-marker and triple-marker models as diagnostic indicators of PDAC. (H) ROC curves of sCD58, TGF-β1, dual-marker and triple-marker models as diagnostic indicators of PDAC in CA199 diagnosis failure. ****p<0.0001. AUC, area under the curve; PDAC, pancreatic ductal adenocarcinoma; ROC, receiver operator characteristic.

of 516 serum samples were analyzed. The AUC of sCD58, TGF-β1, and CA199 were 0.801, 0.834, and 0.836, respectively (figure 8D). According to the maximum Youden index, the optimal cut-off values for sCD58, TGF-β1, and lgCA199+1 were 298.7 ng/mL, 1001.0 pg/mL, and 2.7, respectively (online supplemental Figure 8G-I). ROC curves for commonly used clinical tumor markers are shown in online supplemental Figure 8J). Among them, AUC values, confidence intervals, optimal cut-off values, sensitivity, and specificity were summarized in online supplemental Table S5. These findings suggested that either sCD58 or TGF-β1 possesses excellent diagnostic value and may be a good surrogate for CA19-9. Meanwhile, we generated the dual-marker model (sCD58+TGF-β1) and triple-marker model (sCD58+TGF-β1+CA199) by logistic regression fitting (see Methods). The data showed that the AUC of the triple-marker model of sCD58+TGF-β1+CA199 was 0.946, superior to the dual-marker model and CA199 alone (figure 8G). For diagnostic specificity and sensitivity, CA19-9 was characterized by high specificity (94.12%), but low sensitivity (67.97%) in diagnosing PDAC. Of note, the triple-marker model could increase the sensitivity to 81.05% while maintaining the specificity unchanged (online supplemental Table S6). Therefore, the triple-marker model significantly improved PDAC detection accuracy and reduced missed diagnoses compared with single biomarkers.

Furthermore, we assessed the diagnostic efficacy of sCD58, TGF-β1, and the combined models when CA199 failed. Elevated CA19-9 in PDAC (n=108) and normal CA199 in non-PDAC (n=272) were excluded. The remaining 79 patients with CA19-9 misdiagnosis were further analyzed, including normal CA19-9 in PDAC (n=45) and elevated CA199 in non-PDAC (n=34). The results demonstrated that the AUC of sCD58, TGF-β1, dual-marker, and triple-marker models were 0.880, 0.890,

Table 1 Relationship between serum sCD58 and clinicopathological characteristics in PDAC patients (N=171)

Parameters	Total	Serum sCD58		P value
		Low (n=86)	High (n=85)	
Age (years)				0.248
<60	91	42	49	
≥60	80	44	36	
Gender				0.484
Female	77	41	36	
Male	94	45	49	
Tobacco use				0.380
No	118	62	56	
Yes	53	24	29	
Alcohol use				0.571
No	126	65	61	
Yes	45	21	24	
Diabetes				0.829
No	116	59	57	
Yes	55	27	28	
Hypertension				0.119
No	113	52	61	
Yes	58	34	24	
Tumor location				0.680
Head	106	52	54	
Body/tail	65	34	31	
Histological grade				0.647
G1	20	12	8	
G2	89	44	45	
G3	62	30	32	
Tumor size (cm)				**0.026***
≤4	120	67	53	
> 4	51	19	32	
Lymph node metastasis				0.066
Negative	64	38	26	
Positive	107	48	59	
Distant metastasis				**0.043***
No	153	81	72	
Yes	18	5	13	
TNM stage				**0.011***
I-IIA	58	37	21	
IIB-IV	113	49	64	
Perineural invasion				0.096
Negative	74	43	31	
Positive	93	42	51	
Missing Values	4	1	3	
Macrovascular invasion				**0.025***
Negative	113	64	49	
Positive	55	21	34	
Missing values	3	1	2	

*p<0.05.
PDAC, pancreatic ductal adenocarcinoma.

0.955, and 0.740, respectively (figure 8H, online supplemental Table S7). These data demonstrated that sCD58 and TGF-β1 retained strong diagnostic performance when CA19-9 fails. The dual-marker model achieved optimal diagnostic ability. However, the diagnostic effect of the triple-marker model notably decreased, which may be caused by the combination of CA199 within this model.

Subsequently, we investigated the prognostic value of serum sCD58 in patients with PDAC. Of 171 PDAC patients, 43 were unreachable or refused follow-up, leaving 128 patients with complete follow-up data. Of these, 73 died and 55 survived. X-tile software obtained optimal cut-off values for serum sCD58, 370.3 ng/mL. Survival analysis showed that PDAC patients with high serum levels of sCD58 had a shorter overall survival time (p=0.010, figure 8E). Patients with high serum sCD58 had a median survival of 16.8 months, whereas those with low levels reached 40.3 months. However, there was no significant difference regarding TGF-β1 serum levels on survival (online supplemental Figure 8K). In addition, patients with high CA19-9 expression had a worse prognosis (p=0.003, figure 8F).

DISCUSSION

In this study, we first discovered the expressional separation of CD58 of PDAC cells induced by TAMs in the TME. TAMs increase sCD58 production while reducing the mCD58 expression through the TGF-β/smad2/3 signaling pathway. This dual action impedes immune adhesion and recognition by interfering with the CD2-CD58 interaction between T/NK cells and PDAC cells, ultimately facilitating tumor immune evasion and accelerating PDAC progression. This vicious crosstalk between TAMs and T/NK cells is a novel finding to uncover the immunosuppressive networks connecting adaptive and innate immunity in the TIME. More importantly, serum circulating sCD58 may serve as a promising biomarker for the diagnosis and prognosis of PDAC.

Theoretically, as an immune-adhesion membrane protein, CD58 should be predominantly expressed on the cell membrane. IF staining in AsPC-1 and Panc-1 cell lines confirmed membrane localization of CD58, which likely represents the molecular basis for its primary biological function. However, we also observed cytoplasmic expression of CD58 in Panc-1 cells and notably detected CD58 accumulation forming distinct "cytoplasmic pool" in PDAC tissues. Consistent with our findings, Autschbach *et al*[40] directly observed CD58 staining in both membrane

and cytoplasm of hepatocytes in chronic hepatitis under electron microscopy. The intensity of staining was positively correlated with the degree of inflammatory activity. Kirby *et al*[41] found a similar phenomenon that tumor cells contained a certain amount of CD58 in the cytoplasm. We speculate that cytoplasmic CD58 (cCD58) may assume different functional roles from mCD58. This differential subcellular localization likely reflects dynamic equilibrium among cCD58, mCD58, and sCD58 isoforms, though the precise molecular mechanisms warrant further investigation. Moreover, the cell type-specific distribution patterns of CD58 in AsPC-1 versus Panc-1 cells further underscore the cellular heterogeneity characteristic of PDAC.

The CD2-CD58 axis promotes cell adhesion and participates in lymphocyte activation and effector functions, including cytolytic activity against tumor cells.[42 43] Loss of CD58 may lead to evasion of immune surveillance by CTLs and NK cell-mediated cytolysis.[44–47] Recent studies have shown that intact CD58 expression and linkage with CD2 in cancer cells are necessary for antitumor immunity, strengthening the stability of PD-L1 protein.[43] Intriguingly, CD58 expression is elevated in PDAC tissues compared with normal pancreatic tissues.[34] Consistent with our previous findings, multiple research teams have found that CD58 expression is increased in colorectal cancer and glioblastoma.[48–51] Paradoxically, elevated CD58 appears to be more conducive for immune cells to recognize and kill through the CD2-CD58 axis. Combined with the previously reported existence of fluid CD58,[31] we believe that sCD58 may be an important cause of the contradiction. Speculatively, sCD58 may act as a counter-receptor to competitively bind to CD2 to inhibit the roles of mCD58 and further suppress the activation of T/NK cells. Afterward, we further analyzed its roles in the TIME.

TAMs are the main immune cell population in the TIME, with diverse phenotypes and functions that induce immunosuppression, promote tumor progression, and predict poor survival.[16 52] In this study, PDAC-induced TAMs displayed an M2-like phenotype. Further, TAMs can induce the expressional separation of CD58 in PDAC cells. Considering that PDAC cells can induce a high-level production of TGF-β in TAMs, we tested the roles of TGF-β to induce the expressional separation of CD58. Through in-depth mining, we found a positive correlation between CD58 and TGF-β/smad2/3 pathway in PDAC. However, it is noteworthy that CD58 was reduced at the protein level in PDAC cells after indirect co-culture with TAMs, although the TGF-β/smad2/3 pathway was activated. For this discordant phenomenon, we hypothesized that the reduction of mCD58 at the protein level was likely to be related to sCD58 production. Subsequent experiments corroborated this hypothesis, activation of TGF-β/Smad2/3 signaling was accompanied by decreased mCD58 on the cell membrane and increased sCD58 in the supernatant of PDAC cells after indirect co-culture. However, the exact mechanism of sCD58 production remains unclear and needs further analysis. It is conceivable that there is shedding of the membrane protein CD58 by specific enzymes and subsequent release of the soluble form, which results in an increase of the soluble form sCD58 accompanied by a decrease of the membrane form mCD58.[53] Alternatively, alternative splicing of mRNA leads to the production of truncated CD58 lacking intracellular or transmembrane domains, which are directly transported and secreted into the extracellular space after synthesis.

CD2, the natural ligand for mCD58, is localized in T/NK cells and binds with high affinity to mCD58 on target cells.[42 54] CD2-mCD58 interaction is a major adhesion pathway between T cells and target cells, as well as a key costimulatory pathway for T/NK cell activation.[55 56] Our data confirmed a positive rate of CD2 on the surface of T/NK cells as nearly 100%. Defects in CD2-CD58 axis confer immune evasion from CAR-T cell and T-cell engagers mediated antitumor efficacy by the inhibition of cell expansion, cytokine secretion, degranulation, and cytotoxicity, while potentiating PD-L1 protein stabilization.[43 46 57] CMTM6 is critical for the stability of CD58 and for the upregulation of PD-L1 in the absence of CD58.[43] Loss of CD58 dampens T cell-tumor interactions and response to PD-1/PD-L1 blockade.[58] Competition between CD58 and PD-L1 for CMTM6 binding maintains the balance of expression in these two immune checkpoint ligands with opposing functions.[43 58] Resistance to ICB is an important challenge in cancer therapy.[59] Deficiency of CD58 in melanoma from patients with ICB resistance leads to immune evasion, without affecting the expression of major histocompatibility complex, indicating that its effect is different from the known mechanism of ICB resistance.[60] However, the role of sCD58 in the TIME remained to be illustrated. Subcutaneous tumor-bearing models and intraperitoneal xenograft models warranted that mCD58 increases the activation ratio of T/NK cells and enhances T/NK cytotoxicity, while sCD58 inhibits the activation and cytotoxicity of T/NK cells. Mechanistically, mCD58 enhances the immune adhesion and recognition of T/NK cells via CD2-CD58 interaction, thereby stimulating T/NK cell activation, boosting their cytotoxicity, and promoting cytokine release to support antitumor immunity. On the other side, high concentrations of sCD58 in the TME competitively bind the CD2 on the surface of T/NK cells as a pseudomolecule to block the CD2-CD58 axis. This interference impairs T/NK-cell activation, attenuates their cytotoxicity and cytokine secretion, and fosters the formation of an immunosuppressive TIME, ultimately propelling PDAC immune escape.

Notably, the positive rate of CD58 in murine PDAC cell suspensions was more than 80% and even 90% before inoculation of xenografts. This high rate decreased dramatically after 4 weeks of subcutaneous tumor inoculation, to only less than 20%, and did not maintain the high positive rate and high expression of CD58. This was likely due to the fact that the inoculated cell suspension was a polyclonal cell population, PDAC cells with high CD58 expression were more likely to be attacked by T/NK cells after subcutaneous inoculation into immunocompetent mice, making PDAC cells with relatively low CD58 expression more likely to survive. Thus, it eventually led to a dramatic reduction in the positive rate of CD58 in the detected PDAC cell population. High local concentrations of sCD58 protected PDAC cells

by competitively blocking CD2-CD58 interaction, thereby impairing T/NK-cell recognition and cytotoxicity.

Existing studies provide limited data on serum sCD58 levels and their prognostic value in solid tumors. Hoffmann *et al*[61] found an increase in sCD58 levels in malignant pleural effusion of lung cancer. Here, we investigated the differences in serum sCD58 levels between PDAC patients and healthy controls. The sCD58 content was significantly increased in the serum of PDAC patients and correlated with tumor size, distant metastasis, TNM stage, and macrovascular invasion. This indicates that the growth of PDAC may lead to the release of high concentrations of sCD58 into the blood through infiltrating blood vessels. Our data further suggested that serum sCD58 has potential value in predicting the prognosis of PDAC patients. CA199 is the only relevant biomarker to diagnose PDAC in the routine clinical setting. However, jaundice, pancreatitis, and Lewis antigen expression interfere with its power. In this study, we constructed a combined diagnostic model consisting of CA199, TGF-β1, and sCD58, which has the highest AUC of 0.946. Even in the CA199 misdiagnosed patients, the combined diagnostic model of TGF-β1 and sCD58 has an AUC of 0.955. These data revealed the potential of serum sCD58 as a biomarker for PDAC in a clinical setting.

There are several limitations in this study. First, the exact molecular mechanisms of expressional separation of CD58 need to be addressed in subsequent analysis. Second, the clinical significance of sCD58 should be further validated in independent PDAC cohorts.

CONCLUSIONS

The expressional separation of CD58 acts as a novel crosstalk between TAMs and T/NK cells in the TIME of PDAC, connecting the adaptive and innate immune systems to induce immunosuppression. These results present a novel target for immunotherapy. Furthermore, serum sCD58 has the potential to serve as a biomarker to improve the diagnostic accuracy of CA19-9 and predict the prognosis of PDAC patients.

Author affiliations
[1]Department of General Surgery, The First Affiliated Hospital of USTC, Division of Life Science and Medicine, University of Science and Technology of China, Hefei, Anhui, People's Republic of China
[2]Department of General Surgery, Peking Union Medical College Hospial, Beijing, People's Republic of China
[3]Department of Gastrointestinal Surgery, Shandong Provincial Hospital Affiliated to Shandong First Medical University, Jinan, People's Republic of China
[4]Department of Gastrointestinal Surgery, Shandong Provincial Hospital, Shandong University, Jinan, People's Republic of China
[5]Department of Visceral, Vascular and Endocrine Surgery, Martin-Luther-University Halle-Wittenberg, Halle, Germany

Contributors YZ, HZ and RZ contributed equally to this study. YZ, HZ and RZ were involved in the conception of the study. YZ, HZ, RZ, JL, SY and YZ performed the experiments. YZ and HZ drafted the original manuscript. JK, QLia and QLiu revised the manuscript. QLia and QLiu provided funding and supervision. All authors read and approved the final manuscript. All authors approved the submission to this journal. Guarantor: QLiu is the guarantor of this study and accepts full responsibility. Use ChatGPT for language polishing to improve the language of the article.

Funding This study was supported by the National Natural Science Foundation of China (82172765, 82303272, 82373230, 82373289), Anhui Provincial Natural Science Foundation (2308085QH275), China Postdoctoral Science Foundation (2023M733393); National High-Level Hospital Clinical Research Funding (2022-PUMCH-D-001); CAMS Innovation Fund for Medical Sciences (2023-I2M-C&T-B024; 2024-I2M-ZD-001; CIFMS, 2023-I2M-2-002); Peking Union Medical College Hospital Outstanding Young Talent Development Program (No. UBJ11020).

Competing interests No, there are no competing interests.

Patient consent for publication Not applicable.

Ethics approval This study involves human participants and was approved by the Ethics Committee of Peking Union Medical College Hospital (No. JS-2954). Participants gave informed consent to participate in the study before taking part. The animal models used in this study were based on C57BL/6 immunocompetent mice or NSG (NOD.Cg-*Prkdc*^{scid}*Il2rg*^{em1Smoc}) immunodeficient mice (6–8 weeks old). All of the animal experiments were approved by the Animal Ethics Committee of Peking Union Medical College Hospital (XHDW-2021-042). The whole process was implemented in strict accordance with the specifications of the Regulations of the Administration of Laboratory Animals in China to reduce animal fear and pain and protect the welfare of laboratory animals. All mice were bred under SPF conditions and acclimatized to the new environment for 1 week to minimize stress.

Provenance and peer review Not commissioned; externally peer reviewed.

Data availability statement Data are available on reasonable request. Data are available on reasonable request. All data relevant to the study are included in the article or uploaded as supplementary information.

ORCID iD
Huaijin Zheng http://orcid.org/0009-0009-6425-3019

REFERENCES

1 Stoop TF, Javed AA, Oba A, *et al*. Pancreatic cancer. *Lancet* 2025;405:1182–202.
2 Bray F, Laversanne M, Sung H, *et al*. Global cancer statistics 2022: GLOBOCAN estimates of incidence and mortality worldwide for 36 cancers in 185 countries. *CA Cancer J Clin* 2024;74:229–63.
3 Hu ZI, O'Reilly EM. Therapeutic developments in pancreatic cancer. *Nat Rev Gastroenterol Hepatol* 2024;21:7–24.
4 Piersma B, Hayward MK, Weaver VM. Fibrosis and cancer: A strained relationship. *Biochim Biophys Acta Rev Cancer* 2020;1873:188356.
5 Bärthel S, Falcomatà C, Rad R, *et al*. Single-cell profiling to explore pancreatic cancer heterogeneity, plasticity and response to therapy. *Nat Cancer* 2023;4:454–67.
6 Liu Q, Liao Q, Zhao Y. Chemotherapy and tumor microenvironment of pancreatic cancer. *Cancer Cell Int* 2017;17:68.
7 Wang X, Hu L-P, Qin W-T, *et al*. Identification of a subset of immunosuppressive P2RX1-negative neutrophils in pancreatic cancer liver metastasis. *Nat Commun* 2021;12:174.
8 Pan Y, Yu Y, Wang X, *et al*. Tumor-Associated Macrophages in Tumor Immunity. *Front Immunol* 2020;11:583084.
9 De Sanctis F, Lamolinara A, Boschi F, *et al*. Interrupting the nitrosative stress fuels tumor-specific cytotoxic T lymphocytes in pancreatic cancer. *J Immunother Cancer* 2022;10:e003549.
10 Fu L-Q, Du W-L, Cai M-H, *et al*. The roles of tumor-associated macrophages in tumor angiogenesis and metastasis. *Cell Immunol* 2020;353:104119.

11 Chu X, Tian Y, Lv C. Decoding the spatiotemporal heterogeneity of tumor-associated macrophages. *Mol Cancer* 2024;23:150.
12 Sun D, Luo T, Dong P, *et al*. M2-polarized tumor-associated macrophages promote epithelial-mesenchymal transition via activation of the AKT3/PRAS40 signaling pathway in intrahepatic cholangiocarcinoma. *J Cell Biochem* 2020;121:2828–38.
13 Beatty GL, Chiorean EG, Fishman MP, *et al*. CD40 agonists alter tumor stroma and show efficacy against pancreatic carcinoma in mice and humans. *Science* 2011;331:1612–6.
14 Nywening TM, Wang-Gillam A, Sanford DE, *et al*. Targeting tumour-associated macrophages with CCR2 inhibition in combination with FOLFIRINOX in patients with borderline resectable and locally advanced pancreatic cancer: a single-centre, open-label, dose-finding, non-randomised, phase 1b trial. *Lancet Oncol* 2016;17:651–62.
15 Michaels AD, Newhook TE, Adair SJ, *et al*. CD47 Blockade as an Adjuvant Immunotherapy for Resectable Pancreatic Cancer. *Clin Cancer Res* 2018;24:1415–25.
16 Liu Q, Wu H, Li Y, *et al*. Combined blockade of TGf-β1 and GM-CSF improves chemotherapeutic effects for pancreatic cancer by modulating tumor microenvironment. *Cancer Immunol Immunother* 2020;69:1477–92.
17 O'Kane GM, Wang YQ, Gonzalez R, *et al*. 1309P CD8+ T cell infiltration is associated with improved survival in advanced pancreatic cancer. *Ann Oncol* 2022;33:S1142.
18 Li HB, Yang ZH, Guo QQ. Immune checkpoint inhibition for pancreatic ductal adenocarcinoma: limitations and prospects: a systematic review. *Cell Commun Signal* 2021;19:117.
19 Giurini EF, Ralph O, Pappas SG, *et al*. Looking Beyond Checkpoint Inhibitor Monotherapy: Uncovering New Frontiers for Pancreatic Cancer Immunotherapy. *Mol Cancer Ther* 2025;24:18–32.
20 Kunk PR, Bauer TW, Slingluff CL, *et al*. From bench to bedside a comprehensive review of pancreatic cancer immunotherapy. *J Immunother Cancer* 2016;4:14.
21 Choi Y, Shi Y, Haymaker CL, *et al*. T-cell agonists in cancer immunotherapy. *J Immunother Cancer* 2020;8:e000966:8:.
22 Jia H, Yang H, Xiong H, *et al*. NK cell exhaustion in the tumor microenvironment. *Front Immunol* 2023;14:1303605.
23 Tumino N, Nava Lauson CB, Tiberti S, *et al*. The tumor microenvironment drives NK cell metabolic dysfunction leading to impaired antitumor activity. *Int J Cancer* 2023;152:1698–706.
24 Shi X, Liu H, Liang Z. Cellular crosstalk of regulatory T cells in pancreatic ductal adenocarcinoma. *Journal of Pancreatology* 2024;7:131–40.
25 Zhou J, Zhang S, Guo C. Crosstalk between macrophages and natural killer cells in the tumor microenvironment. *Int Immunopharmacol* 2021;101:108374.
26 Möller P, Koretz K, Schlag P, *et al*. Frequency of abnormal expression of HLA-A,B,C and HLA-DR molecules, invariant chain, and LFA-3 (CD58) in colorectal carcinoma and its impact on tumor recurrence. *Int J Cancer* 1991;47:155–62.
27 Dustin ML, Selvaraj P, Mattaliano RJ, *et al*. Anchoring mechanisms for LFA-3 cell adhesion glycoprotein at membrane surface. *Nature New Biol* 1987;329:846–8.
28 Bierer BE, Burakoff SJ. T cell adhesion molecules. *FASEB J* 1988;2:2584–90.
29 Dustin ML, Sanders ME, Shaw S, *et al*. Purified lymphocyte function-associated antigen 3 binds to CD2 and mediates T lymphocyte adhesion. *J Exp Med* 1987;165:677–92.
30 Thor Straten P, Garrido F. Targetless T cells in cancer immunotherapy. *J Immunother Cancer* 2016;4:23.
31 Hoffmann JC, Dengler TJ, Knolle PA, *et al*. A soluble form of the adhesion receptor CD58 (LFA-3) is present in human body fluids. *Eur J Immunol* 1993;23:3003–10.
32 Chandrashekar DS, Karthikeyan SK, Korla PK, *et al*. UALCAN: An update to the integrated cancer data analysis platform. *Neoplasia* 2022;25:18–27.
33 Vasaikar SV, Straub P, Wang J, *et al*. LinkedOmics: analyzing multi-omics data within and across 32 cancer types. *Nucleic Acids Res* 2018;46:D956–63.
34 Zhang Y, Liu Q, Liu J, *et al*. Upregulated CD58 is associated with clinicopathological characteristics and poor prognosis of patients with pancreatic ductal adenocarcinoma. *Cancer Cell Int* 2021;21:327.
35 Zhang Y, Liu Q, Yang S, *et al*. Knockdown of LRRN1 inhibits malignant phenotypes through the regulation of HIF-1α/Notch pathway in pancreatic ductal adenocarcinoma. *Mol Ther Oncolytics* 2021;23:51–64.
36 Zhang Y, Liu Q, Liao Q. Long noncoding RNA: a dazzling dancer in tumor immune microenvironment. *J Exp Clin Cancer Res* 2020;39:231.
37 Li B, Lu Y, Zhong M-C, *et al*. Cis interactions between CD2 and its ligands on T cells are required for T cell activation. *Sci Immunol* 2022;7:eabn6373.
38 Jo Y, Sim H-I, Yun B, *et al*. Revisiting T-cell adhesion molecules as potential targets for cancer immunotherapy: CD226 and CD2. *Exp Mol Med* 2024;56:2113–26.
39 Sido B, Otto G, Zimmermann R, *et al*. Modulation of the CD2 receptor and not disruption of the CD2/CD48 interaction is the principal action of CD2-mediated immunosuppression in the rat. *Cell Immunol* 1997;182:57–67.
40 Autschbach F, Meuer SC, Moebius U, *et al*. Hepatocellular expression of lymphocyte function-associated antigen 3 in chronic hepatitis. *Hepatology* 1991;14:223–30.
41 Kirby AC, Cahen P, Porter SR, *et al*. Soluble and cell-associated forms of the adhesion molecule LFA-3 (CD58) are differentially regulated by inflammatory cytokines. *Cell Adhes Commun* 2000;7:453–64.
42 Romain G, Strati P, Rezvan A, *et al*. Multidimensional single-cell analysis identifies a role for CD2-CD58 interactions in clinical antitumor T cell responses. *J Clin Invest* 2022;132:e159402:132:.
43 Ho P, Melms JC, Rogava M, *et al*. The CD58-CD2 axis is co-regulated with PD-L1 via CMTM6 and shapes anti-tumor immunity. *Cancer Cell* 2023;41:1207–21.
44 Smith ME, Marsh SG, Bodmer JG, *et al*. Loss of HLA-A,B,C allele products and lymphocyte function-associated antigen 3 in colorectal neoplasia. *Proc Natl Acad Sci U S A* 1989;86:5557–61.
45 Nouri AM, Smith ME, Crosby D, *et al*. Selective and non-selective loss of immunoregulatory molecules (HLA-A,B,C antigens and LFA-3) in transitional cell carcinoma. *Br J Cancer* 1990;62:603–6.
46 Yan X, Chen D, Ma X, *et al*. CD58 loss in tumor cells confers functional impairment of CAR T cells. *Blood Adv* 2022;6:5844–56.
47 Zeng H, Yu J, Wang H, *et al*. Cancer ATF4-mediated CD58 endocytosis impairs anti-tumor immunity and immunotherapy. *J Transl Med* 2025;23:225.
48 Mayer B, Lorenz C, Babic R, *et al*. Expression of leukocyte cell adhesion molecules on gastric carcinomas: possible involvement of LFA-3 expression in the development of distant metastases. *Int J Cancer* 1995;64:415–23.
49 Kuppner MC, Hamou MF, de Tribolet N. Activation and adhesion molecule expression on lymphoid infiltrates in human glioblastomas. *J Neuroimmunol* 1990;29:229–38.
50 Xu S, Wen Z, Jiang Q, *et al*. CD58, a novel surface marker, promotes self-renewal of tumor-initiating cells in colorectal cancer. *Oncogene* 2015;34:1520–31.
51 Tian Z, Jia W, Wang Z, *et al*. Clinical significance of immune-related antigen CD58 in gliomas and analysis of its potential core related gene clusters. *Heliyon* 2024;10:e29275.
52 Yang S, Wang M, Hua Y, *et al*. Advanced insights on tumor-associated macrophages revealed by single-cell RNA sequencing: The intratumor heterogeneity, functional phenotypes, and cellular interactions. *Cancer Lett* 2024;584:216610.
53 Schmidt-Arras D, Rose-John S. Regulation of Fibrotic Processes in the Liver by ADAM Proteases. *Cells* 2019;8:1226:8:.
54 Moingeon P, Chang HC, Wallner BP, *et al*. CD2-mediated adhesion facilitates T lymphocyte antigen recognition function. *Nature New Biol* 1989;339:312–4.
55 Bierer BE, Hahn WC. T cell adhesion, avidity regulation and signaling: a molecular analysis of CD2. *Semin Immunol* 1993;5:249–61.
56 Leitner J, Herndler-Brandstetter D, Zlabinger GJ, *et al*. CD58/CD2 Is the Primary Costimulatory Pathway in Human CD28-CD8+ T Cells. *J Immunol* 2015;195:477–87.
57 Shen Y, Eng JS, Fajardo F, *et al*. Cancer cell-intrinsic resistance to BiTE therapy is mediated by loss of CD58 costimulation and modulation of the extrinsic apoptotic pathway. *J Immunother Cancer* 2022;10:e004348.
58 Miao B, Hu Z, Mezzadra R, *et al*. CMTM6 shapes antitumor T cell response through modulating protein expression of CD58 and PD-L1. *Cancer Cell* 2023;41:1817–28.
59 Fritz JM, Lenardo MJ. Development of immune checkpoint therapy for cancer. *J Exp Med* 2019;216:1244–54.
60 Frangieh CJ, Melms JC, Thakore PI, *et al*. Multimodal pooled Perturb-CITE-seq screens in patient models define mechanisms of cancer immune evasion. *Nat Genet* 2021;53:332–41.
61 Hoffmann JC, Krüger H, Lührs J, *et al*. Detection of soluble adhesion molecules in pleural effusions. *Chest* 1996;110:107–13.